Predictions for p+Pb Collisions at the LHC

R. Vogt

Lawrence Livermore National Laboratory, Livermore, CA 94551, USA
Physics Department, University of California, Davis, CA 95616, USA

based on arXiv:1301.1335 [hep-ph] (edited by RV)

with members and friends of the JET Collaboration

Contributions from: Javier Albacete *et al.* (rcBK, charged hadrons), Nestor Armesto (jets), Kari Eskola (π^0), Rainer Fries (direct photons), Vasile Topor Pop *et al.* (HIJINGBB̄), Boris Kopeliovich ($R_{p\mathrm{Pb}}$ for produced pions), Kryzstof Kutak (azimuthal difference between jets), Gergeley Barnafoldi *et al.* (cold matter effects on charged hadrons, forward/backward asymmetry), Rudolf Baier *et al.* (forward photons and dileptons), Amir Rezaeian (b-CGC charged hadrons, rcBK photons), Ivan Vitev (cold matter energy loss effects on charged hadrons, π^0, photons), Xin-Nian Wang (charged hadrons), Jianwei Qiu (gauge bosons), Ben-Wei Zhang (jets, gauge bosons), Ziwei Lin (AMPT), Raju Venugopalan *et al.* (IP-Sat), RV (J/ψ)

Caution Regarding *Asymmetric* $p + A$ Collisions

- **$p + A$ is an asymmetric system, when most people refer to $p + A$, it is the same as the fixed-target frame with the projectile proton moving in the direction of positive rapidity with small momentum fractions in the nucleus at $y > 0$**
- **Colliders are different, either the proton or the nucleus can move in the direction of positive rapidity, *i.e.* $p + A$ or $A + p$**
- **Test beam data were Pb+p so most – but not all – of the predictions have been modified to reflect this**

Model Descriptions

Saturation

Saturation: rcBK (A. Rezaeian, J. Albacete *et al*)

Gluon jet production in pA described by k_T-factorization

$$\frac{d\sigma}{dy\, d^2p_T} = \frac{2\alpha_s}{C_F}\frac{1}{p_T^2}\int d^2\vec{k}_T \phi_p^G\left(x_1;\vec{k}_T\right)\phi_A^G\left(x_2;\vec{p}_T-\vec{k}_T\right)$$

Here $x_{1,2} = (p_T/\sqrt{s})e^{\pm y}$ and unintegrated gluon density, $\phi_A^G(x_i;\vec{k}_T)$, is related to color dipole forward scattering amplitude

$$\begin{aligned}\phi_A^G\left(x_i;\vec{k}_T\right) &= \frac{1}{\alpha_s}\frac{C_F}{(2\pi)^3}\int d^2\vec{b}_T\, d^2\vec{r}_T\, e^{i\vec{k}_T\cdot\vec{r}_T}\,\nabla_T^2\mathcal{N}_A\left(x_i;r_T;b_T\right)\\ \mathcal{N}_A\left(x_i;r_T;b_T\right) &= 2\mathcal{N}_F\left(x_i;r_T;b_T\right)-\mathcal{N}_F^2\left(x_i;r_T;b_T\right)\end{aligned}$$

In k_T-factorized approach, both projectile and target have to be at small x so that CGC formalism is applicable to both

rcBK Hybrid Approach

Hybrid models that treat the projectile (forward) with DGLAP collinear factorization and target with CGC methods

Hadron cross section is proportional to $f_g(x_1,\mu_F^2)N_A(x_2,p_T/z)+f_q(x_1,\mu_F^2)N_F(x_2,p_T/z)$ **modulo fragmentation functions**

$$\begin{aligned}\frac{dN^{pA\to hX}}{d\eta d^2p_T} &= \frac{K}{(2\pi)^2}\Big[\int_{x_F}^1\frac{dz}{z^2}[x_1f_g(x_1,\mu_F^2)N_A(x_2,\frac{p_T}{z})D_{h/g}(z,\mu_{\rm Fr})\\ &+ \Sigma_q x_1 f_q(x_1,\mu_F^2)N_F(x_2,\frac{p_T}{z})D_{h/q}(z,\mu_{\rm Fr})]\\ &+ \frac{\alpha_s^{\rm in}}{2\pi^2}\int_{x_F}^1\frac{dz}{z^2}\frac{z^4}{p_T^4}\int_{k_T^2<\mu_F^2}d^2k_Tk_T^2N_F(k_T,x_2)\int_{x_1}^1\frac{d\xi}{\xi}\\ &\times \Sigma_{i,j=q,\bar q,g}w_{i/j}(\xi)P_{i/j}(\xi)x_1f_j(\frac{x_1}{\xi},\mu_F)D_{h/i}(z,\mu_{\rm Fr})\Big]\ .\end{aligned}$$

K factor introduced to incorporate higher order corrections

Inelastic term is multiplied by $\alpha_s^{\rm in}$, different from running α_s in rcBK equation – in hybrid formulation, strong coupling in dilute regime (proton) can differ from that in the dense system (nucleus) but appropriate scale of $\alpha_s^{\rm in}$ cannot be determined without a NNLO calculation

Factorization, renormalization and fragmentation scales assumed to be equal, $\mu_F=\mu_R=\mu_{\rm Fr}$ with $\mu_F=2p_T$, p_T and $p_T/2$ to form uncertainty range for given N and $\alpha_s^{\rm in}$

rcBK Equation

$N_{A(F)}$ **is 2-D Fourier transform of imaginary part of dipole scattering amplitude in the fundamental** (F) **or adjoint** (A) **representation** $\mathcal{N}_{A(F)}$

$\mathcal{N}_{A(F)}$ **calculated using JIMWLK which simplifies to BK in the large** N_c **limit**

Running coupling corrections to LL kernel result in rcBK equation

$$\begin{aligned}\frac{\partial \mathcal{N}_{A(F)}(r,x)}{\partial \ln(x_0/x)} &= \int d^2\vec{r}_1 \; K^{\rm run}(\vec{r},\vec{r}_1,\vec{r}_2)\left[\mathcal{N}_{A(F)}(r_1,x)+\mathcal{N}_{A(F)}(r_2,x)\right.\\ &- \left.\mathcal{N}_{A(F)}(r,x)-\mathcal{N}_{A(F)}(r_1,x)\,\mathcal{N}_{A(F)}(r_2,x)\right]\end{aligned}$$

$$\mathcal{N}(r,Y=0) = 1-\exp\left[-\frac{\left(r^2\,Q_{0s}^2\right)^\gamma}{4}\,\ln\left(\frac{1}{\Lambda\,r}+e\right)\right]$$

Last equation is initial condition with γ **fixed from DIS data,** $\gamma=1$ **is MV initial condition,** $\gamma\sim 1.1$ **in fits**

$Q_{0p}^2\sim 0.2$ **GeV**^{2} **in MV initial condition, smaller for other values of** γ

$Q_{0A}^2\sim NQ_{0p}^2$ **with** $3<N<7$ **in Rezaeian's calculations, Albacete** *et al* **let nuclear scale be proportional to the number of participants at a given** b **to account for geometrical fluctuations in Monte Carlo simulations**

Saturation: IP-Sat (Tribedy and Venugopalan)

Here one starts as before with k_T-factorization

$$\frac{dN_g^{pA}(b_T)}{dy\ d^2p_T} = \frac{4\alpha_s}{\pi C_F}\frac{1}{p_T^2}\int \frac{d^2k_T}{(2\pi)^5}\int d^2s_T \frac{d\phi_p(x_1,k_T|s_T)}{d^2s_T}\frac{d\phi_A(x_2,p_T-k_T|s_T-b_T)}{d^2s_T}$$

Unintegrated gluon density is expressed in terms of the dipole cross section as

$$\frac{d\phi^{p,A}(x,k_T|s_T)}{d^2s_T} = \frac{k_T^2N_c}{4\alpha_s}\int_0^\infty d^2r_T e^{i\vec{k_T}.\vec{r_T}}\left[1-\frac{1}{2}\frac{d\sigma_{\rm dip}^{p,A}}{d^2s_T}(r_T,x,s_T)\right]^2$$

Dipole cross section is a refinement of Golec-Biernat–Wusthoff that gives the right perturbative limit for $r_T \to 0$, equivalent to effective theory of CGC to LL

$$\frac{d\sigma_{\rm dip}^{p}}{d^2b_T}(r_T,x,b_T) = 2\left[1-\exp\left(-\frac{\pi^2}{2N_c}r_T^2\alpha_s(\mu^2)xg(x,\mu^2)T_p(b_T)\right)\right]$$

μ^2 is related to dipole radius, r_T, by $\mu^2 = \frac{4}{r_T^2}+\mu_0^2$

The gluon density $g(x,\mu^2)$ is LO DGLAP result without quarks

$T_p(b_T)$ is the gluon density profile function, $T_p(b_T) = (2\pi B_G)^{-1}\exp\left[-(b_T^2/2B_G)\right]$ where $\langle b^2\rangle = 2B_G$, the average squared gluonic radius of the proton, obtained from HERA data

Event-by-Event Calculations

HIJING2.0 (X.-N. Wang *et al*)

Based on two-component model of hadron production, soft (string excitations with effective cross section $\sigma_{\rm soft}$) and hard (perturbative QCD) components separated by cutoff momentum p_0
LO pQCD calculation with K factor to absorb higher-order corrections

$$\frac{d\sigma_{pA}^{\rm jet}}{dy_1 d^2p_T} = K \int dy_2\, d^2b\, T_A(b) \sum_{a,b,c} x_1 f_{a/p}(x_1, p_T^2) x_2 f_{a/A}(x_2, p_T^2, b) \frac{d\sigma_{ab\to cd}}{dt}$$

Effective $2 \to 2$ scattering, $x_{1,2} = p_T(e^{\pm y_1} + e^{\pm y_2})/\sqrt{s}$

Default HIJING collisions decomposed into independent and sequential NN collisions – in each NN interaction, hard collisions simulated first, followed by soft

Since hard interactions occur over shorter time scale, HIJING2.0 also uses decoherent hard scattering (DHC) where all hard collisions are simulated first, then soft, so available energy unrestricted by soft interactions
Energy-dependent k_T broadening in HIJING

$$\langle k_T^2 \rangle = [0.14 \log(\sqrt{s}/\mathrm{GeV}) - 0.43]\,\mathrm{GeV}^2/c^2 \qquad (1)$$

Shadowing in HIJING

Shadowing treated as scale independent
Versions before HIJING2.0 did not differentiate between quark and gluon shadowing

$$
\begin{aligned}
f_{a/A}(x,\mu_F^2,b) &= S_{a/A}(x,\mu_F^2,b) f_{a/A}(x,\mu_F^2) \\
S_{a/A}(x) &\equiv \frac{f_{a/A}(x)}{A f_{a/N}(x)} \\
&= 1 + 1.19\log^{1/6}\!A\,[x^3 - 1.2x^2 + 0.21x] \\
&\quad -s_a(A^{1/3}-1)^n\left[1 - \frac{10.8}{\log(A+1)}\sqrt{x}\right] e^{-x^2/0.01} \\
s_a(b) &= s_a\frac{5}{3}\Big(1 - \frac{b^2}{R_A^2}\Big)
\end{aligned}
$$

In HIJING2.0 the $(A^{1/3}-1)$ factor is nonlinear ($n = 0.6$) but $n = 1$ in earlier versions

Previously $s_a = s_g = s_q = 0.1$

In HIJING2.0 $s_g \neq s_q$: $s_q = 0.1$ and $s_g \sim 0.22 - 0.23$ to match LHC data

The b dependence of s_a gives some impact parameter dependence to $S_{a/A}$

HIJINGB$\overline{\text{B}}$ (V. Topor Pop *et al*)

Differs from standard HIJING in treatment of fragmentation

HIJING uses string fragmentation with constant vacuum value of $\kappa_0 = 1.0$ GeV/fm for string tension

HIJINGB$\overline{\text{B}}$ allows for multiple overlapping flux tubes leading to strong longitudinal color field (SCF) effects

SCF effects modeled by varying κ and momentum cutoff with $\sqrt{s}$ and A

Fragmentation also modified, including baryon loops to explain baryon to meson anomaly and increase strange baryon production

AMPT: A Multi-Phase Transport (Z. Lin)

AMPT is a Monte Carlo transport model for heavy ion collisions, montage of other codes

- Heavy Ion Jet Interaction Generator (HIJING) for generating the initial conditions
- Zhang's Parton Cascade (ZPC) for modeling partonic scatterings
- A Relativistic Transport (ART) model for treating hadronic scatterings

AMPT – def treats the initial condition as strings and minijets and using Lund string fragmentation

AMPT – SM treats the initial condition as partons and uses a simple coalescence model to describe hadronization

Perturbative QCD Calculations

Leading Order Calculations (I. Vitev *et al*)

LO single inclusive hadron production cross section

$$\frac{d\sigma}{dyd^2p_T} = K\frac{\alpha_s^2}{s}\sum_{a,b,c}\int\frac{dx_1}{x_1}d^2k_{T_1}\,f_{a/N}(x_1,k_{T_1}^2)\int\frac{dx_2}{x_2}d^2k_{T_2}\,f_{b/N}(x_2,k_{T_2}^2)$$
$$\times\int\frac{dz_c}{z_c^2}\,D_{h/c}(z_c)H_{ab\to c}(\hat{s},\hat{t},\hat{u})\delta(\hat{s}+\hat{t}+\hat{u})$$

Gaussian form of k_T dependence in parton densities assumed

$$f_{a/N}(x_1,k_{T_1}^2) = f_{a/N}(x_1)\frac{1}{\pi\langle k_T^2\rangle}e^{-k_{T_1}^2/\langle k_T^2\rangle}$$

In pp collisions, $\langle k_T^2\rangle_{pp} = 1.8$ GeV$^2/c^2$

Broadening increased in cold matter, $\langle k_T^2\rangle_{pA} = \langle k_T^2\rangle_{pp} + \langle 2\mu^2 L/\lambda_{q,g}\rangle\zeta$

Cold matter energy loss due to medium-induced gluon Bremsstrahlung, implemented as a shift in momentum fraction, $f_{i/p}(x) \longrightarrow f_{i/p}(x/(1-\epsilon_{i,\mathrm{eff}}))$ where $\epsilon \propto \Sigma_i\Delta E_i/E$ with the sum over all medium-induced gluons

Dynamical shadowing shifts nuclear parton momentum fraction so that $f_{i/p}(x) \longrightarrow f_{i/p}((x/-\hat{t})(1+C_i\zeta_i^2(A^{1/3}-1))$

Proton and neutron number (isospin) accounted for

Initial-State Shadowing (G. Barnafoldi *et al*)

`kTpQCD_v2.0` assumes collinear factorization up to NLO

$$
\begin{aligned}
E_h \frac{d\sigma_h^{pp}}{d^3p_T} &= \frac{1}{s}\sum_{abc}\int_{VW/z_c}^{1-(1-V)/z_c}\frac{dv}{v(1-v)}\int_{VW/vz_c}^{1}\frac{dw}{w}\int^1 dz_c \\
&\times \int d^2\vec{k}_{T_1}\int d^2\vec{k}_{T_2}\; f_{a/p}(x_1,\vec{k}_{T_1},\mu_F^2)\, f_{b/p}(x_2,\vec{k}_{T_2},\mu_F^2) \\
&\times \left[\frac{d\tilde{\sigma}}{dv}\delta(1-w) + \frac{\alpha_s(\mu_R)}{\pi}K_{ab,c}(\hat{s},v,w,\mu_F,\mu_R,\mu_{\rm Fr})\right]\frac{D_c^h(z_c,\mu_{\rm Fr}^2)}{\pi z_c^2}\ .
\end{aligned}
$$

$d\tilde{\sigma}/dv$ is LO cross section with next-order correction term $K_{ab,c}(\hat{s},v,w,\mu_F,\mu_R,\mu_{\rm Fr})$

Proton and parton level NLO kinematic variables are (s, V, W) and ($\hat{s}$, v, w)

k_T broadening implemented similar to previous LO calculation with

$$
\begin{aligned}
\langle k_T^2\rangle_{pA} &= \langle k_T^2\rangle_{pp} + C h_{pA}(b) \\
h_{pA}(b) &= \begin{cases} \nu_A(b)-1 & \nu_A(b)<\nu_m \\ \nu_m - 1 & \text{otherwise}\end{cases}
\end{aligned}
$$

Shadowing implemented through available parameterizations: EKS98, EPS08, HKN, and `HIJING2.0` − scale dependence included

$$
f_{a/A}(x,\mu_F^2) = S_{a/A}(x,\mu_F^2)\left[\frac{Z}{A}f_{a/p}(x,\mu_F^2) + \left(1-\frac{Z}{A}\right)f_{a/n}(x,\mu_F^2)\right]
$$

Charged Particle Multiplicity and p_T Distributions: Midrapidity

$dN_{\rm ch}/d\eta$ Center-of-Mass vs Lab Frame

Most calculations done in CM Frame, shift to lab frame involves a shift of $\Delta y_{NN} = 0.465$ in the direction of the proton beam

Results in lab frame only shown for calculations when directly available from the source

Test run data do not favor saturation results

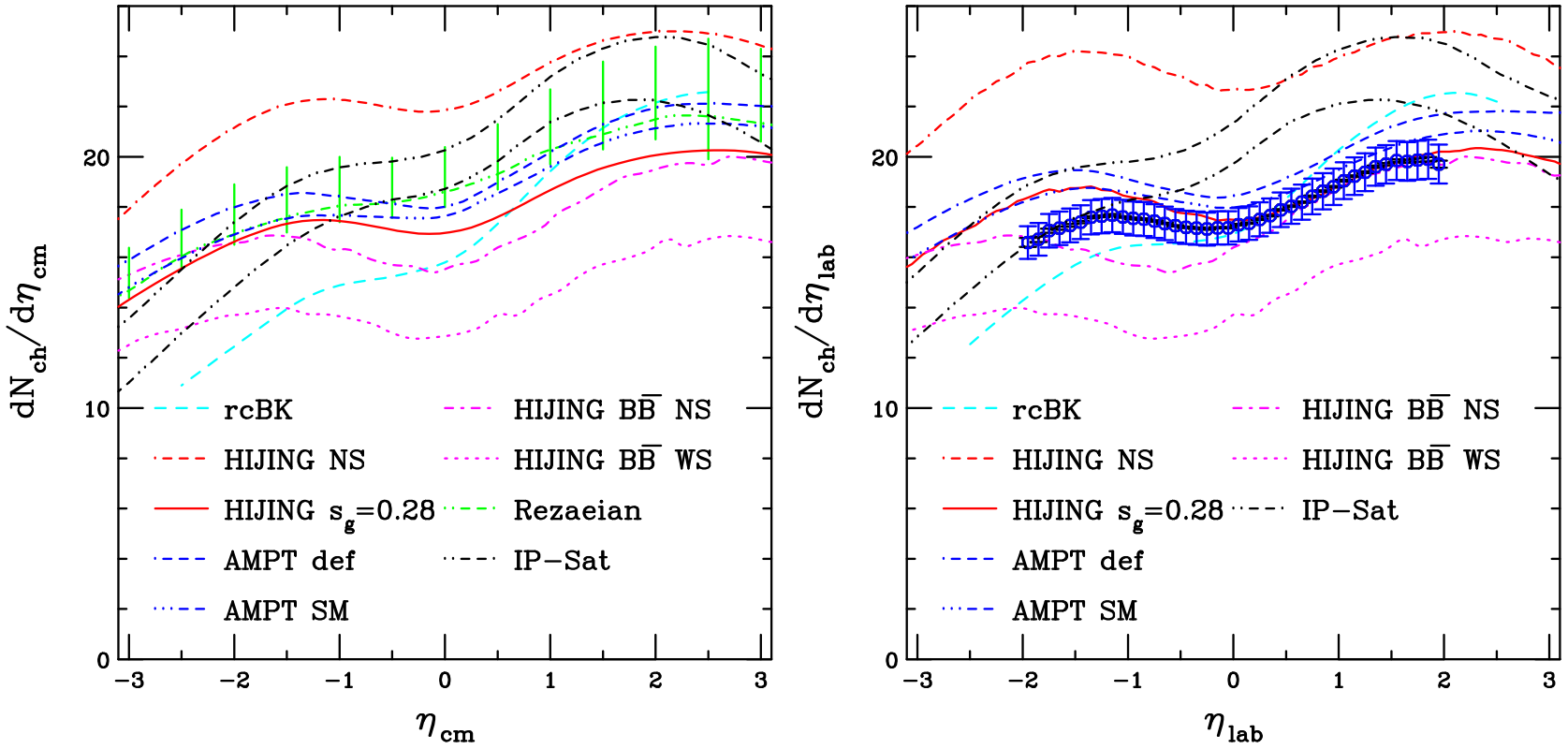

Figure 1: **Charged particle pseudorapidity distributions at $\sqrt{s_{NN}} = 5.02$ TeV in the CM (left) and lab (right) frames. Courtesy of Albacete *et al.*, XN Wang *et al.*, Z Lin, Rezaeian, and Topor Pop *et al.*.**

Relative p and Pb Peak Ratios in Lab Frame

Models without saturation come closer to data as well as getting the forward/backward ratio right

	$dN_{\rm ch}/d\eta_{\rm lab}$			$R(\eta_{\rm lab}=2/\eta_{\rm lab}=-2)$
	-2	**0**	**2**	
ALICE	16.65 ± 0.65	17.24 ± 0.66	19.81 ± 0.78	1.19 ± 0.05
Saturation Models				
IP-Sat	**17.55**	**20.55**	**23.11**	**1.32**
KLN	**15.96**	**17.51**	**22.02**	**1.38**
rcBK	**14.27**	**16.94**	**22.51**	**1.58**
HIJING-based				
2.1 NS (no shad)	**23.58**	**22.67**	**24.96**	**1.06**
2.1 WS ($s_g = 0.28$)	**18.30**	**17.49**	**20.21**	**1.10**
$B\overline{B}$ **NS***	**20.03**	**19.68**	**23.24**	**1.16**
$B\overline{B}$ **NS**†	**16.84**	**16.39**	**19.68**	**1.16**
$B\overline{B}$ **WS***	**12.97**	**12.09**	**15.16**	**1.17**
$B\overline{B}$ **WS**†	**13.98**	**13.71**	**16.73**	**1.20**
AMPT				
Default	**19.07**	**18.56**	**21.65**	**1.14**
String Melting	**18.14**	**18.10**	**20.84**	**1.15**
DPMJET	**17.50**	**17.61**	**20.67**	**1.18**

Table 1: **Comparison of values of $dN_{\rm ch}/d\eta_{\rm lab}$ at $\eta_{\rm lab} = -2$, 0, 2 and the ratio $dN_{\rm ch}/d\eta_{\rm lab}|_{\eta_{\rm lab=2}}/dN_{\rm ch}/d\eta_{\rm lab}|_{\eta_{\rm lab=-2}}$, denoted by R above. The $*$ on HIJING $B\overline{B}$ indicates that the calculations have been shifted to the lab frame by the ALICE Collaboration while the † are results provided by V. Topor Pop. Adapted from ALICE Collaboration, arXiv:1210.3615 [nucl-ex].**

Centrality Dependence of $dN_{\rm ch}/d\eta$

Comparing AMPT (Z. Lin) with b-CGC (A. Rezaeian)

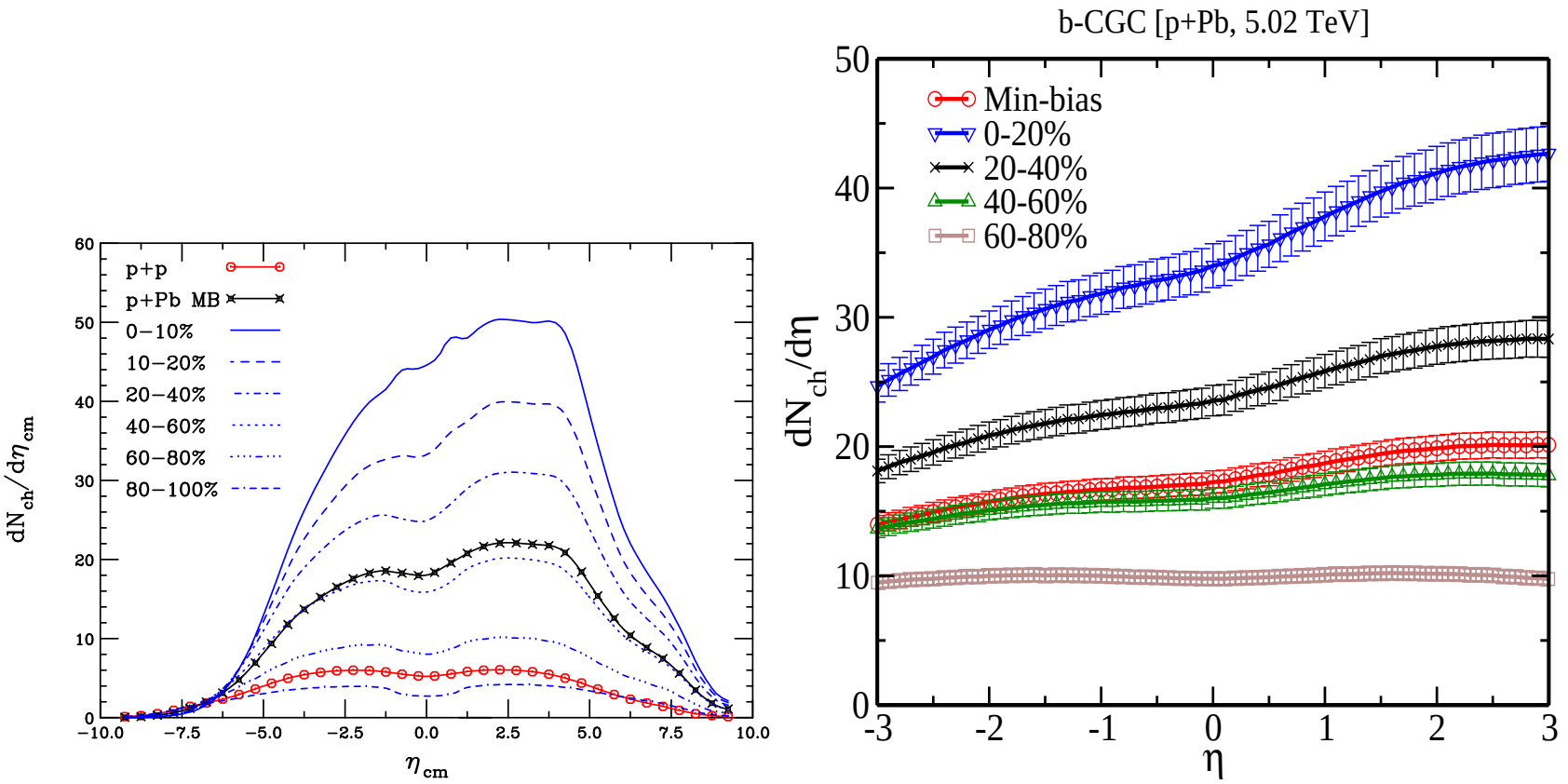

Figure 2: **Charged particle pseudorapidity distributions in the center of mass frame of p+Pb collisions at various centralities for AMPT (left) and within the b-CGC saturation model (right).**

Charged Particle p_T Distributions

Results similar at low p_T but deviate significantly at higher p_T
rcBK distributions do not differ strongly between $\eta = 0$ and 2

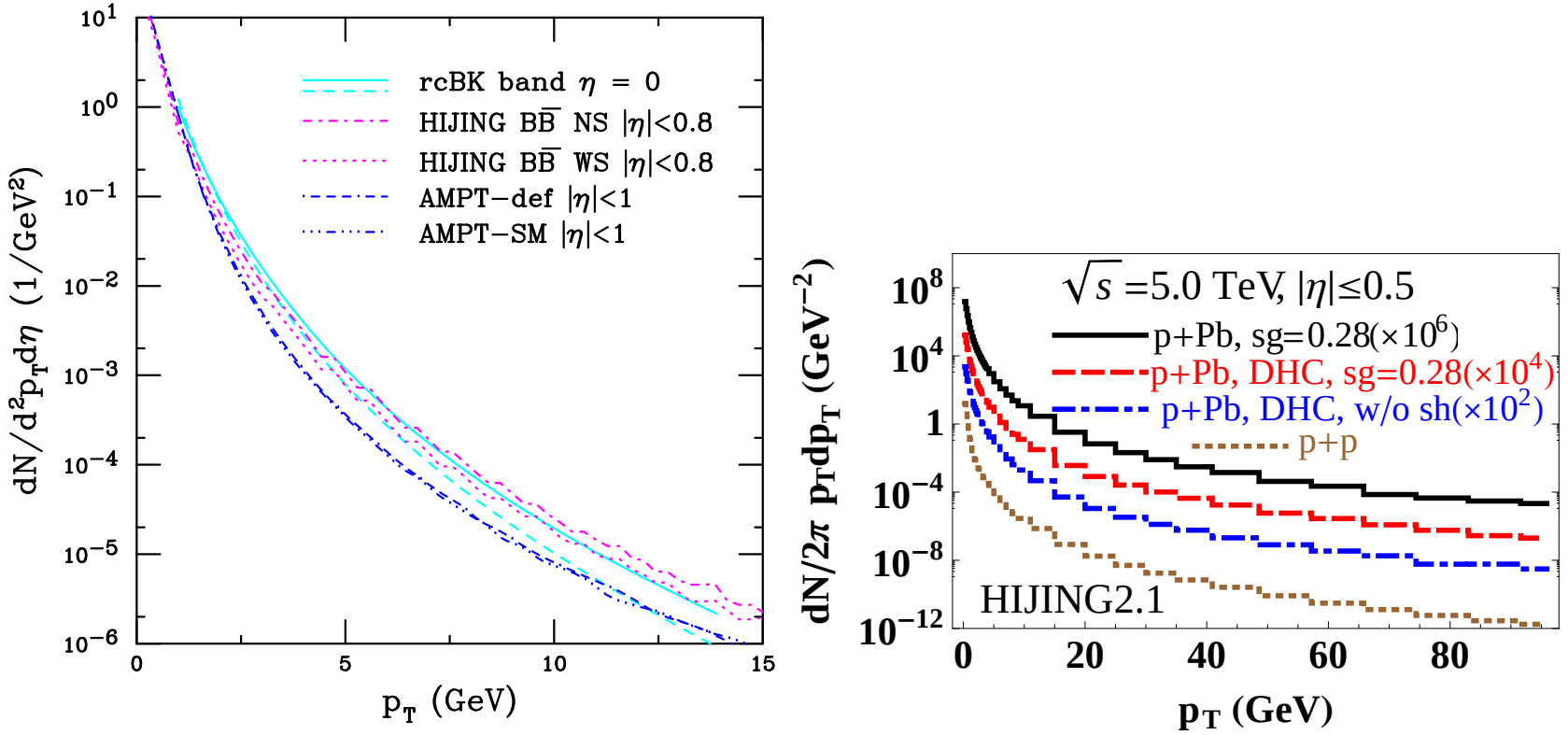

Figure 3: **(Left) Charged particle p_T distributions at $\sqrt{s_{NN}} = 5.02$ TeV. The solid and dashed cyan curves outline the rcBK band calculated by Albacete *et al.*. The magenta curves, calculated with HIJINGBB̄2.0 are presented without (dot-dashed) and with (dotted) shadowing. The AMPT results are given by the dot-dash-dash-dashed (default) and dot-dot-dot-dashed (SM) blue curves. (Right) The charged hadron p_T distribution in p+Pb collisions with different HIJING2.1 options, scaled by the indicated factors to separate the curves. The $p+p$ distribution is shown for comparison.**

Results from the p+Pb Test Run

ALICE $R_{p\mathrm{Pb}}$ data uses pp reference obtained by interpolating between data at 2.76 and 7 TeV, R_{pA} is formed by comparing $|\eta_{\mathrm{lab}}| < 0.8$ in p+Pb to $-0.3 < \eta_{\mathrm{cm}} < 1.3$; calculation of $\eta_{\mathrm{cm}} = \eta_{\mathrm{lab}} + 0.465$ is accurate for $m \sim 0$ or high p_T

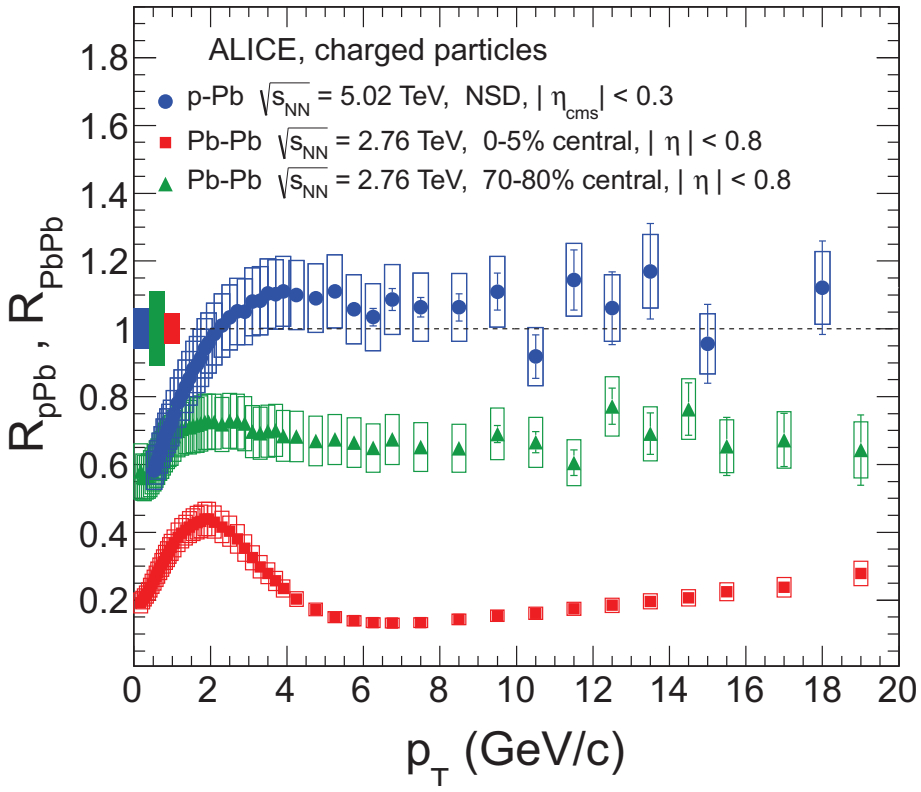

Figure 4: The minimum bias $R_{p\mathrm{Pb}}$ ratio is compared to central and peripheral values of R_{AA} (left) and various models (right). From ALICE Collaboration, arXiv:1210.4520 [nucl-ex].

$R_{p\mathrm{Pb}}$ at Midrapidity: Saturation

Large bands for saturation predictions (rcBK, Albacete and Rezaeian; IP-Sat, Tribedy and Venugopalan)

LO Vitev result includes Cronin effect, cold matter energy loss, and shadowing, difference is whether parameters change with $\sqrt{s}$ or not

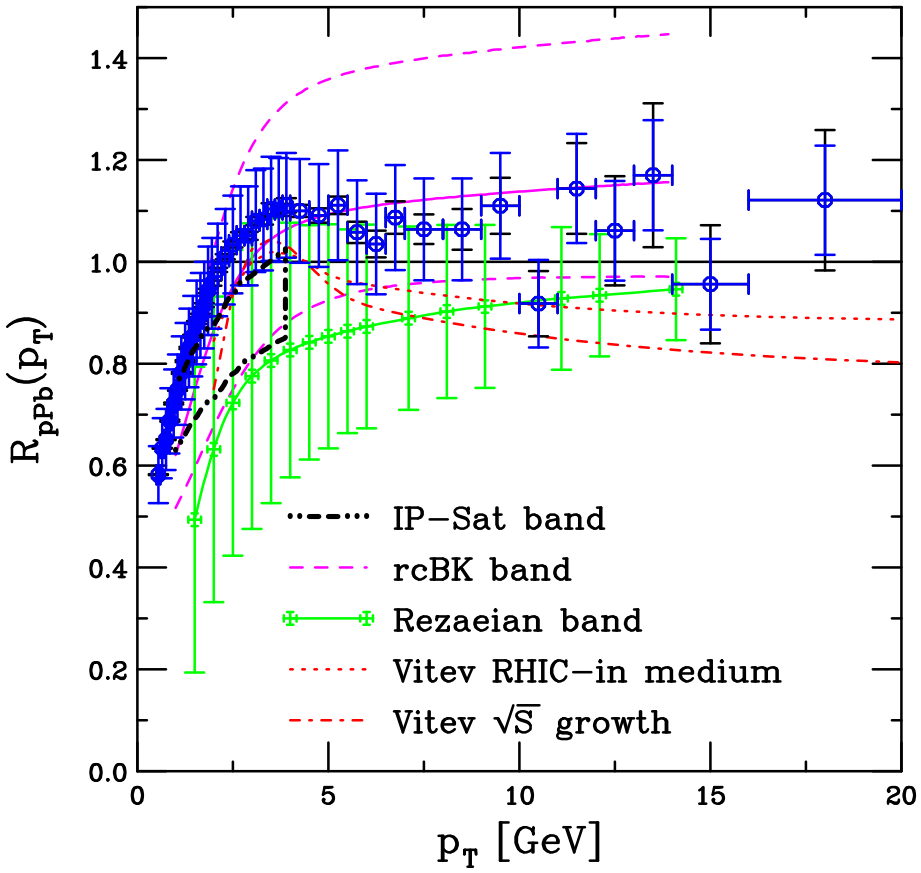

Figure 5: **Charged particle $R_{p\mathrm{Pb}}p_T$ at $\sqrt{s_{NN}} = 5.02$ TeV at $\eta \sim 0$. The bands from saturation models by Albacete *et al.* and Rezaeian (rcBK) and Tribedy & Venugopalan (IP-Sat) are compared to a cold matter calculation by Vitev and collaborators.**

$R_{p\mathrm{Pb}}$ at Midrapidity: Shadowing and HIJING2.0

Standard shadowing parameterizations predict small effect with little p_T dependence

HIJING2.0 stronger than all others, especially at high p_T

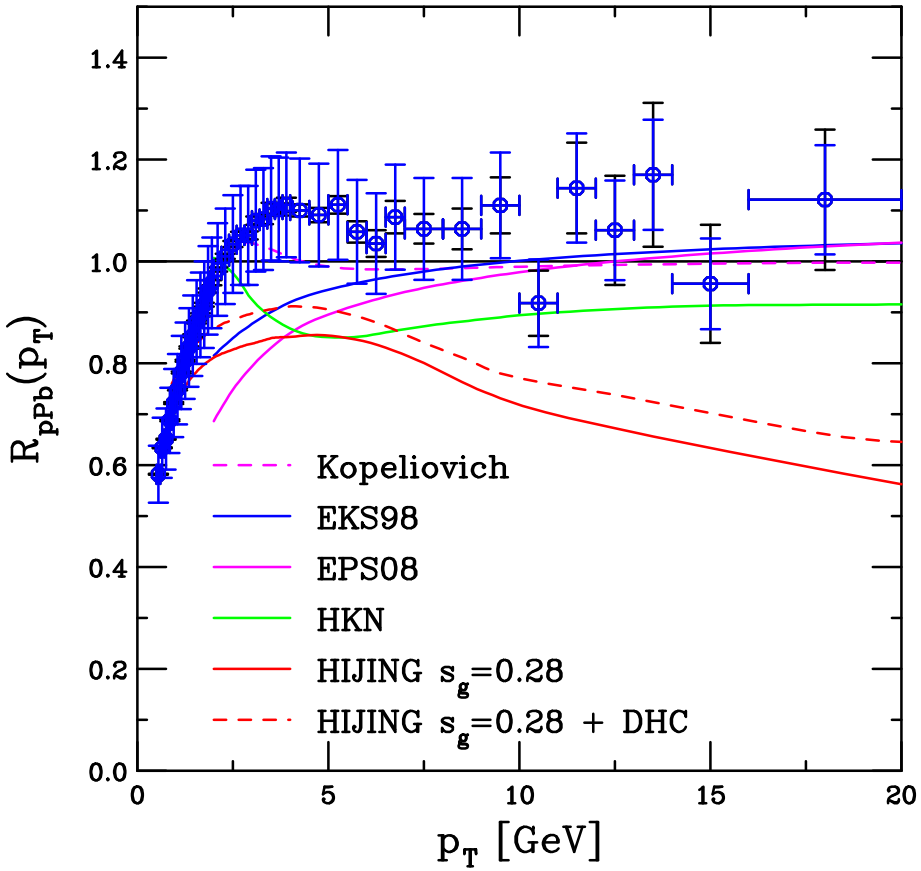

Figure 6: **Charged particle $R_{p\mathrm{Pb}}p_T$ at $\sqrt{s_{NN}} = 5.02$ TeV at $\eta \sim 0$. Results with more 'standard' shadowing (Barnafoldi *et al.*, Kopeliovich) are compared. The difference in the HIJING curves depends on whether the hard scatterings are coherent or not.**

$R_{p\mathrm{Pb}}$ at Midrapidity: Generators

HIJINGBB̄ shows large differences in $R_{p\mathrm{Pb}}$ due to shadowing but AMPT modes do not differ much

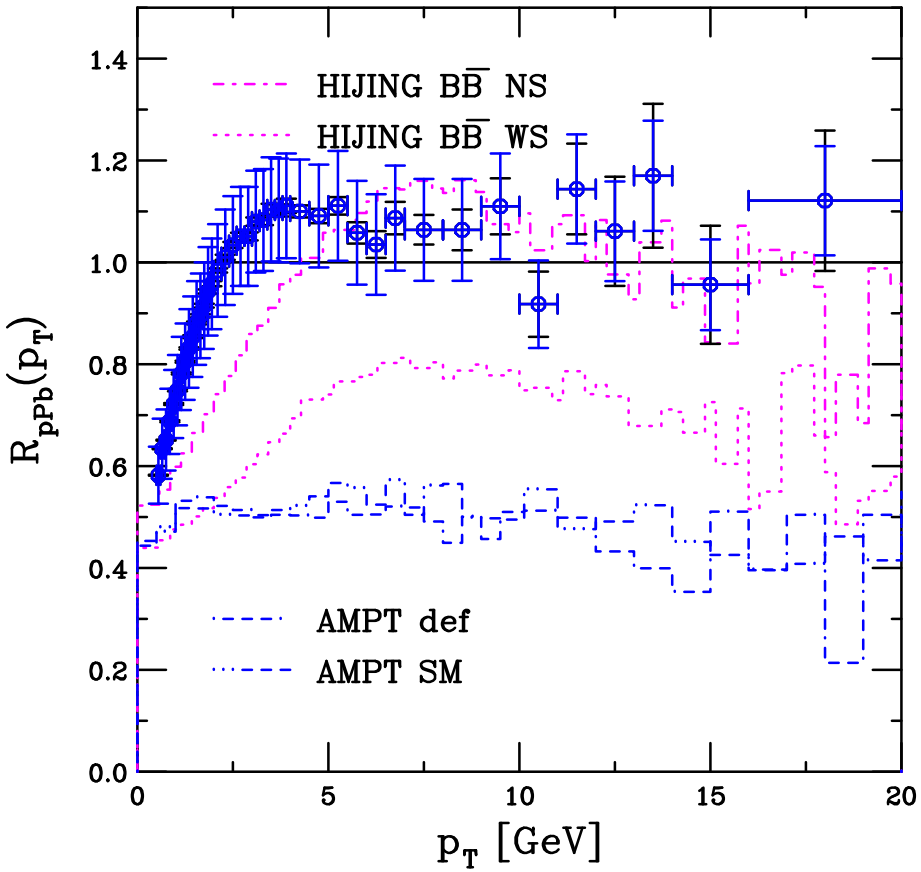

Figure 7: **Charged particle $R_{p\mathrm{Pb}}p_T$ at $\sqrt{s_{NN}} = 5.02$ TeV at $\eta \sim 0$. HIJINGBB̄ (Topor Pop *et al.*) with and without shadowing compared to AMPT (Z. Lin) default and with string melting.**

Charged Particle Multiplicity and p_T Distributions: $\eta \neq 0$

$R_{p\mathrm{Pb}}$ at Midrapidity: parton vs. hadrons in HIJING

Large to small Cronin enhancement seen for parton $R_{p\mathrm{Pb}}$

Hadronization reduces enhancement, decoherent scattering mitigates strong shadowing at high p_T, arrow on right-hand plot indicates the direction that HIJING prediction should go if scale evolution of shadowing is included

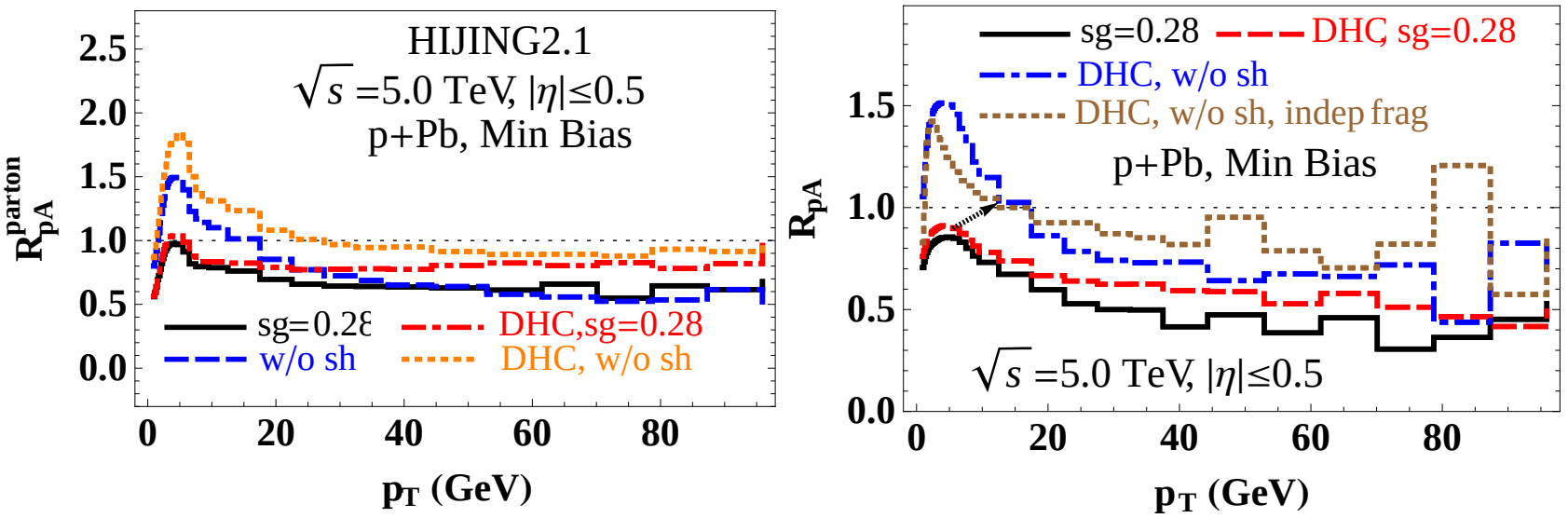

Figure 8: **(Left) The nuclear modification factor of the parton p_T spectra in p+Pb collisions. (Right) The charged hadron nuclear modification factor with different HIJING2.1 options. The arrow indicates the most probable trend of the nuclear modification factor to transition from the low to the high p_T regions.**

Rezaeian rcBK Rapidity Dependence

Results are shown for different N and $\alpha_s^{\rm in}$, along with band for scale uncertainty – fixing N from data at one rapidity will fix it for other rapidities as well

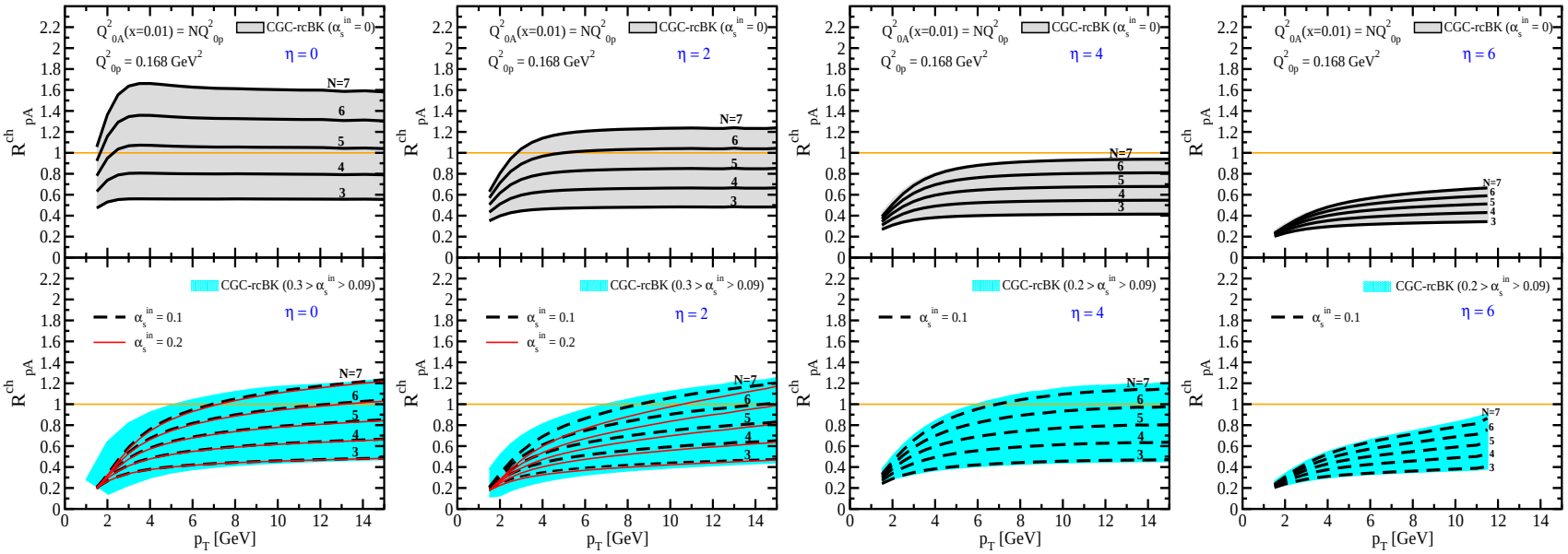

Figure 9: The nuclear modification factor $R_{pA}^{\rm ch}$ for charged hadron production in minimum bias p+Pb collisions at $\eta = 0$, 2, 4, and 6 (with the convention that the proton beam moves toward forward rapidity) obtained from hybrid factorization assuming different values of the saturation scale in the nucleus, Q_{0A}^2. The lines labeled by a given value of N, for $3 < N < 7$, are results with fixed factorization scale $\mu_F = p_T$ and fixed saturation scale $Q_{0A}^2 = NQ_{0p}^2$ and $Q_{0p}^2 = 0.168$ GeV$^2/c^2$. The bands shown the variation in the results with the choice of factorization scale. Two panels are shown for each rapidity. The upper panel shows results obtained by taking $\alpha_s^{in} = 0$ (assuming only elastic contribution) while the bottom panel shows the variation of $\alpha_s^{\rm in}$ in the range $0.09 \geq \alpha_s^{in} \geq 0.3$. In the bottom panels for $\eta = 0$ and 2, results with both $\alpha_s^{\rm in} = 0.1$ and 0.2 are shown, while for $\eta = 4$ and 6, only $\alpha_s^{\rm in} = 0.1$ is shown. The plots are courtesy of Amir Rezaeian.

Albacete *et al* rcBK

Comparison between min bias and two different centralities in p+Pb collisions are shown for $\eta = 0$ and 2

Uncertainty is largest for min bias, weakest effect (and smallest uncertainty) is for peripheral collisions, $N_{\rm part} < 5$

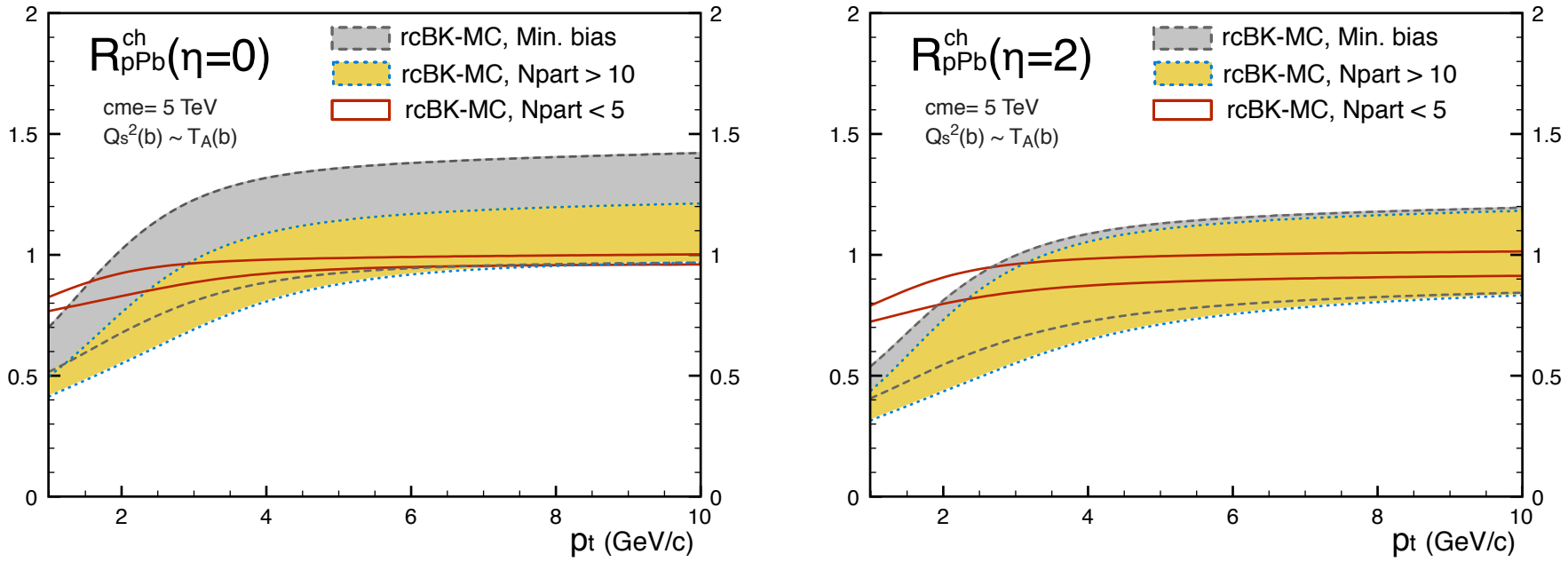

Figure 10: The nuclear modification factor for three different centrality classes assuming k_T-factorization. The $\eta = 2$ result is obtained with the convention that the proton beam moves toward forward rapidity.

Vitev et al Cold Matter Effects

Range of band results from taking the same scattering parameters as at RHIC (upper edge) as well as assuming some enhancement due to the higher energy of the LHC (lower edge)

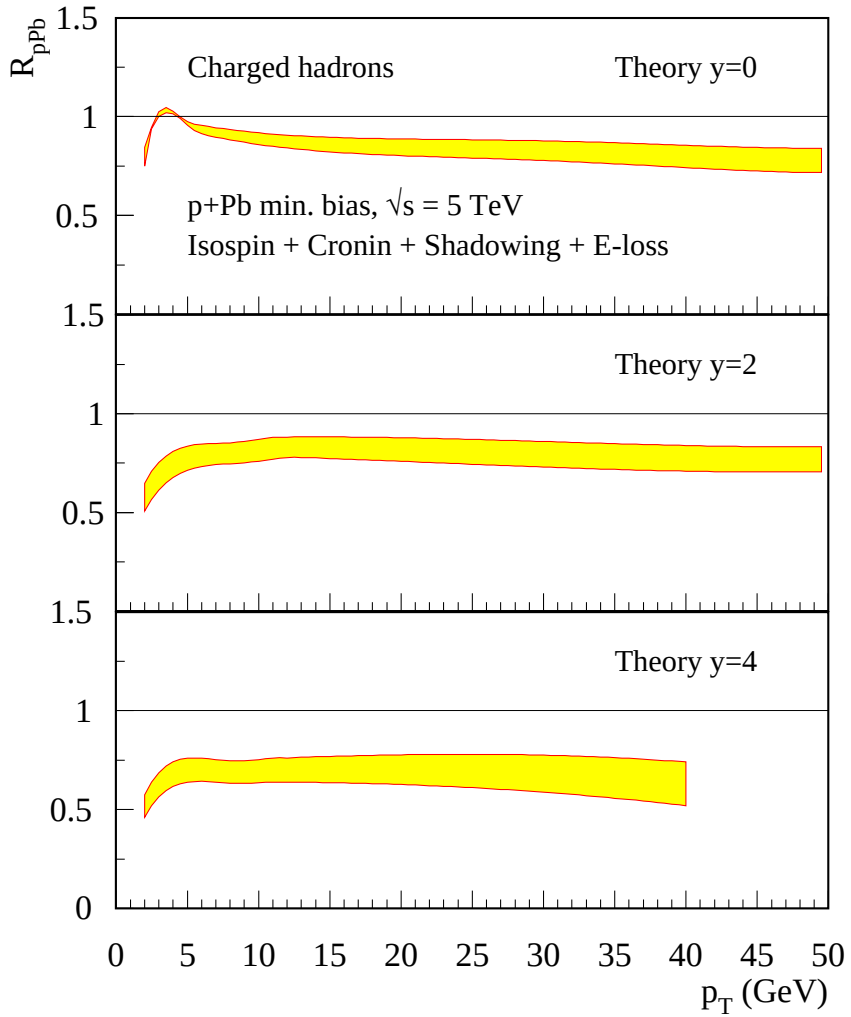

Figure 11: Predictions for the nuclear modification factor R_{pPb} as a function of p_T for charged hadron production in minimum bias p+Pb collisions. Results are shown for three rapidities: $y = 0$ (top), $y = 2$ (center), and $y = 4$ (bottom) with the convention that the proton beam moves toward forward rapidity.

Forward-Backward Asymmetry

$$Y^h_{\rm asym}(p_T) = \frac{E_h d^3\sigma^h_{p\rm Pb}/d^2p_T d\eta|_{\eta>0}}{E_h d^3\sigma^h_{p\rm Pb}/d^2p_T d\eta|_{\eta<0}} = \frac{R^h_{p\rm Pb}(p_T,\eta>0)}{R^h_{p\rm Pb}(p_T,\eta<0)}$$

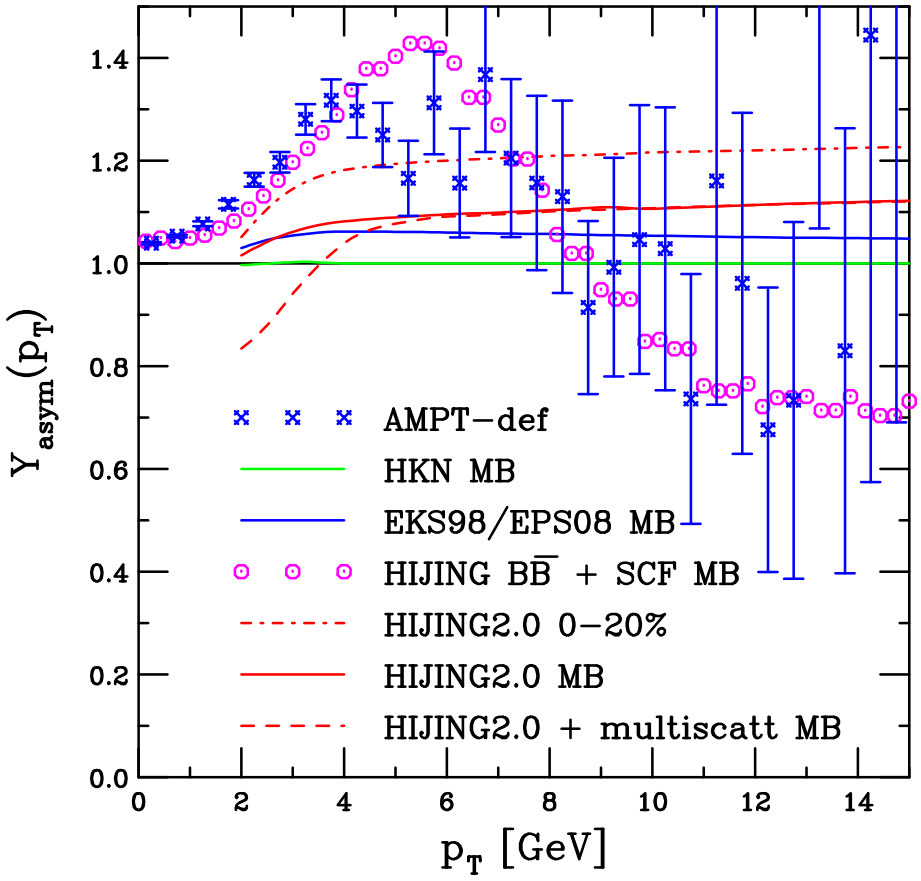

Figure 12: Predictions for the forward-backward asymmetry, $Y^h_{\rm asym}(p_T)$. Centrality independent results are shown for the HKN, EKS98 and EPS08 parameterizations (labeled MB). Minimum bias results are also shown for HIJINGB$\bar{\rm B}$2.0 and HIJING2.0 with multiple scattering. In addition, HIJING2.0 results in MB collisions and for the 20% most central collisions are also shown. The blue points are the AMPT − def results. Courtesy of G. Barnafoldi *et al.*

Identified Particles

$R_{p\mathrm{Pb}}$ for Neutral Pions

EPS09 shadowing + isospin gives enhancement at $y = 0$, including Cronin and energy loss results in reduction

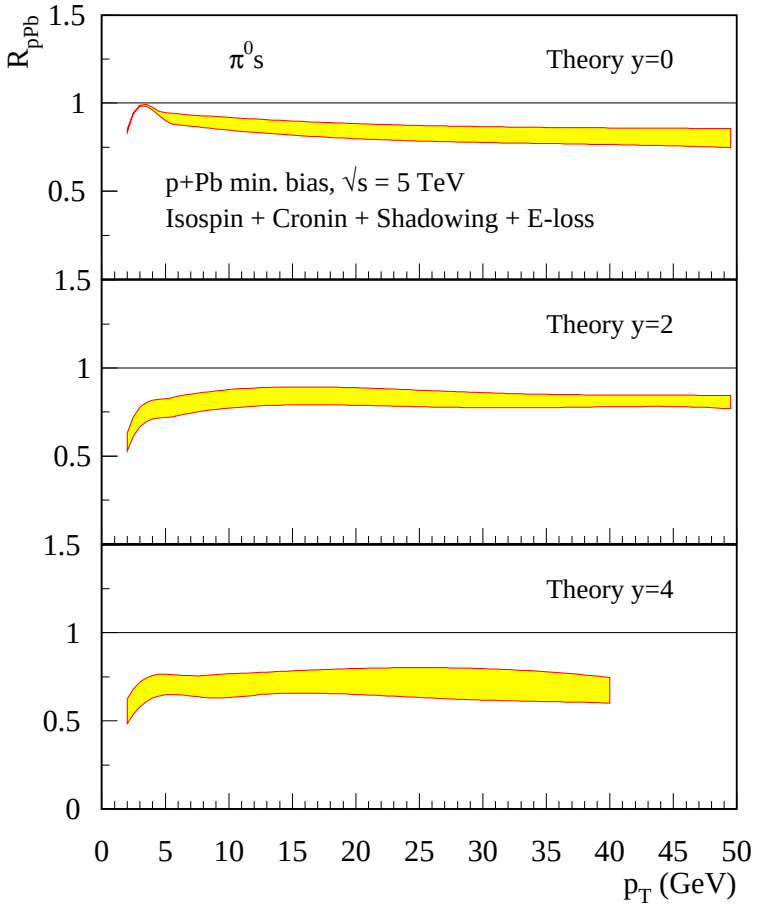

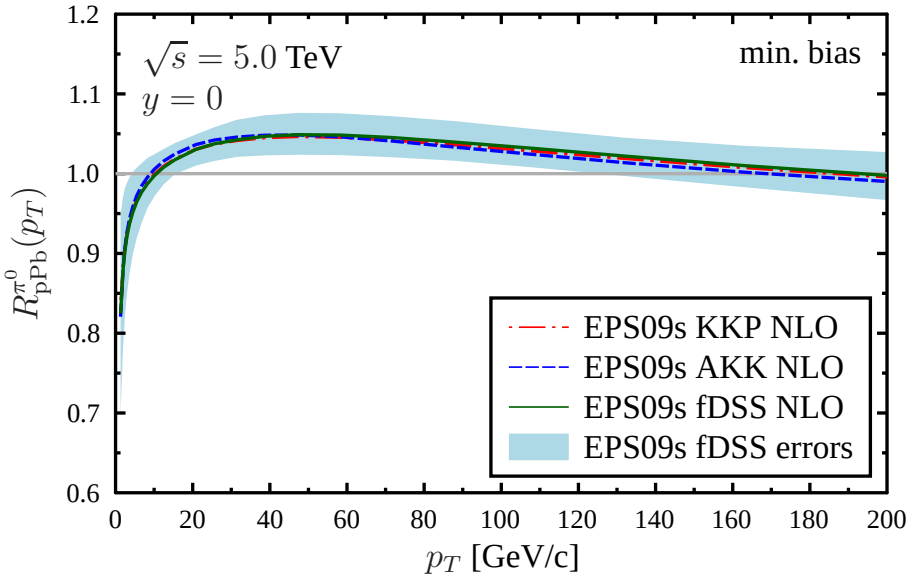

Figure 13: (Left) Vitev *et al.* predictions at $y = 0$, 2 and 4. (Right) Eskola *et al.* comparing different fragmentation functions as well as delineating the EPS09s uncertainties.

AMPT $K^{\pm}$, p, $\overline{p}$ Rapidity Distributions

Definite differences between protons and antiprotons, especially in the direction of motion of the lead nucleus, K^+ and K^- more similar

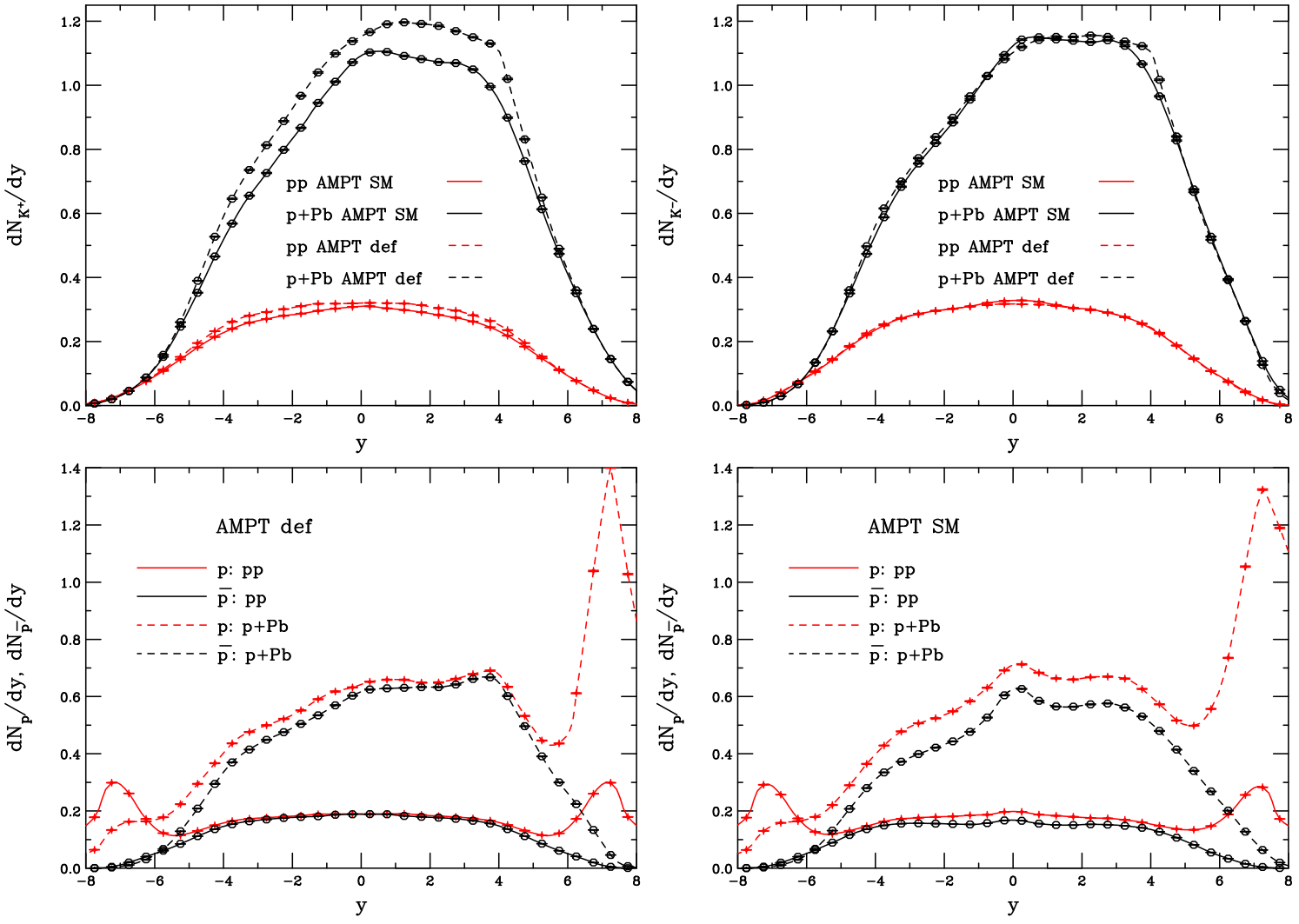

Figure 14: **Rapidity distribution, dN/dy, of K^+ (top left) and K^- (top right) mesons and p (bottom left) and $\overline{p}$ (bottom right) baryons.**

Jets

Multiple Jet Production in Different Rapidity Intervals

NLO jet cross sections and yields for one, two and three jets

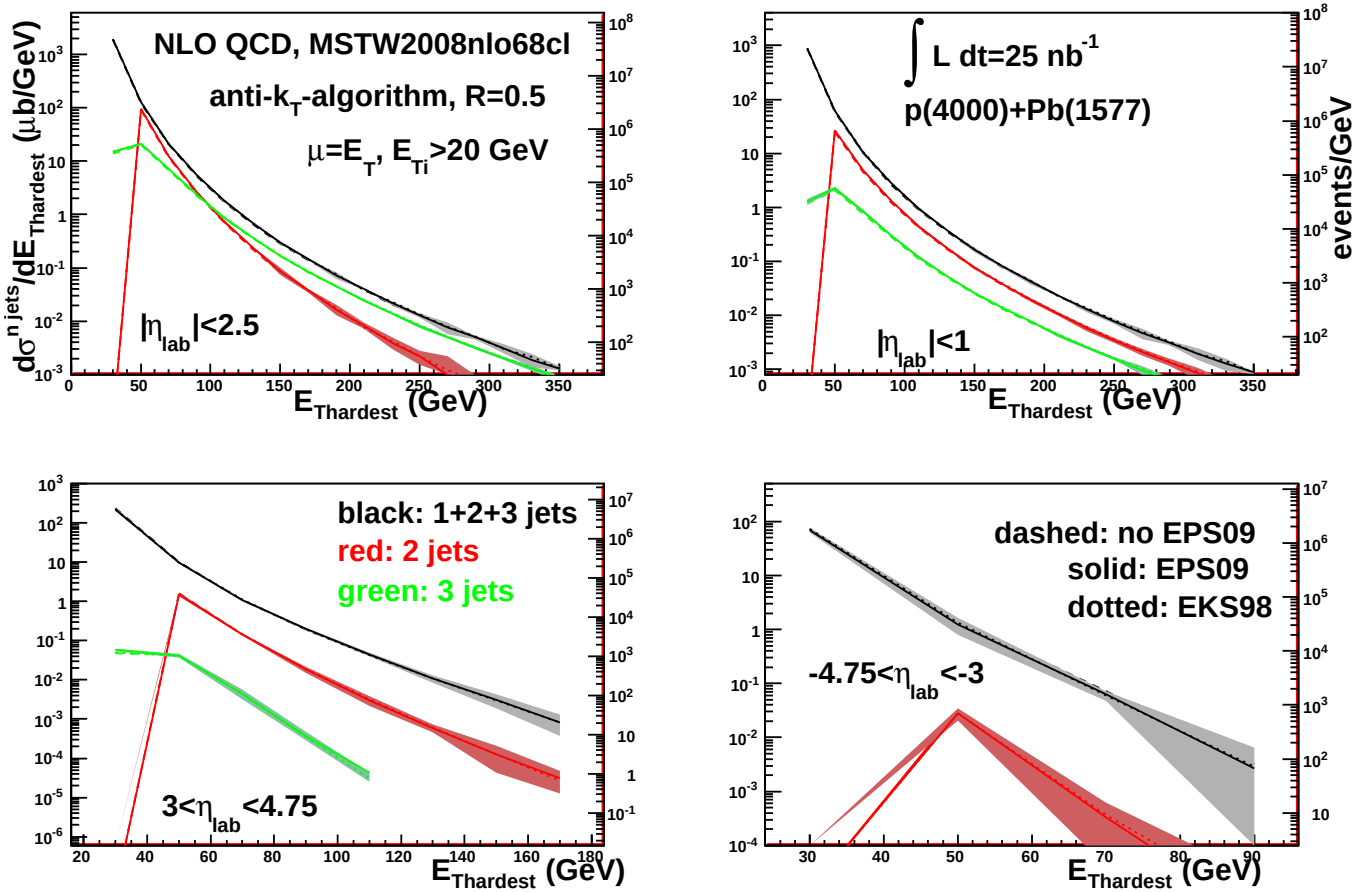

Figure 15: **Sum of the one, two and three jets (black), two jets (red) and three jets (green) cross sections as a function of the E_T of the hardest jet within the acceptance. Different pseudorapidity windows (in the lab frame) computed for minimum bias p+Pb collisions at the LHC (4+1.58 TeV per nucleon) are considered. Dashed lines are the results without nuclear modification to the PDFs; solid lines are the results with EPS09NLO; dotted lines are results with EKS98. The bands correspond to the EPS09 uncertainties. The right-hand y-axes give the corresponding yields for an integrated luminosity of 25 nb^{-1}. Courtesy of Nestor Armesto.**

Cold Matter Effects on Single and Dijet Production

Cold matter jet $R_{p\mathrm{Pb}}$ small (NLO calculation at midrapidity, jet cone $R = 0.4$, not a strong function of E_T

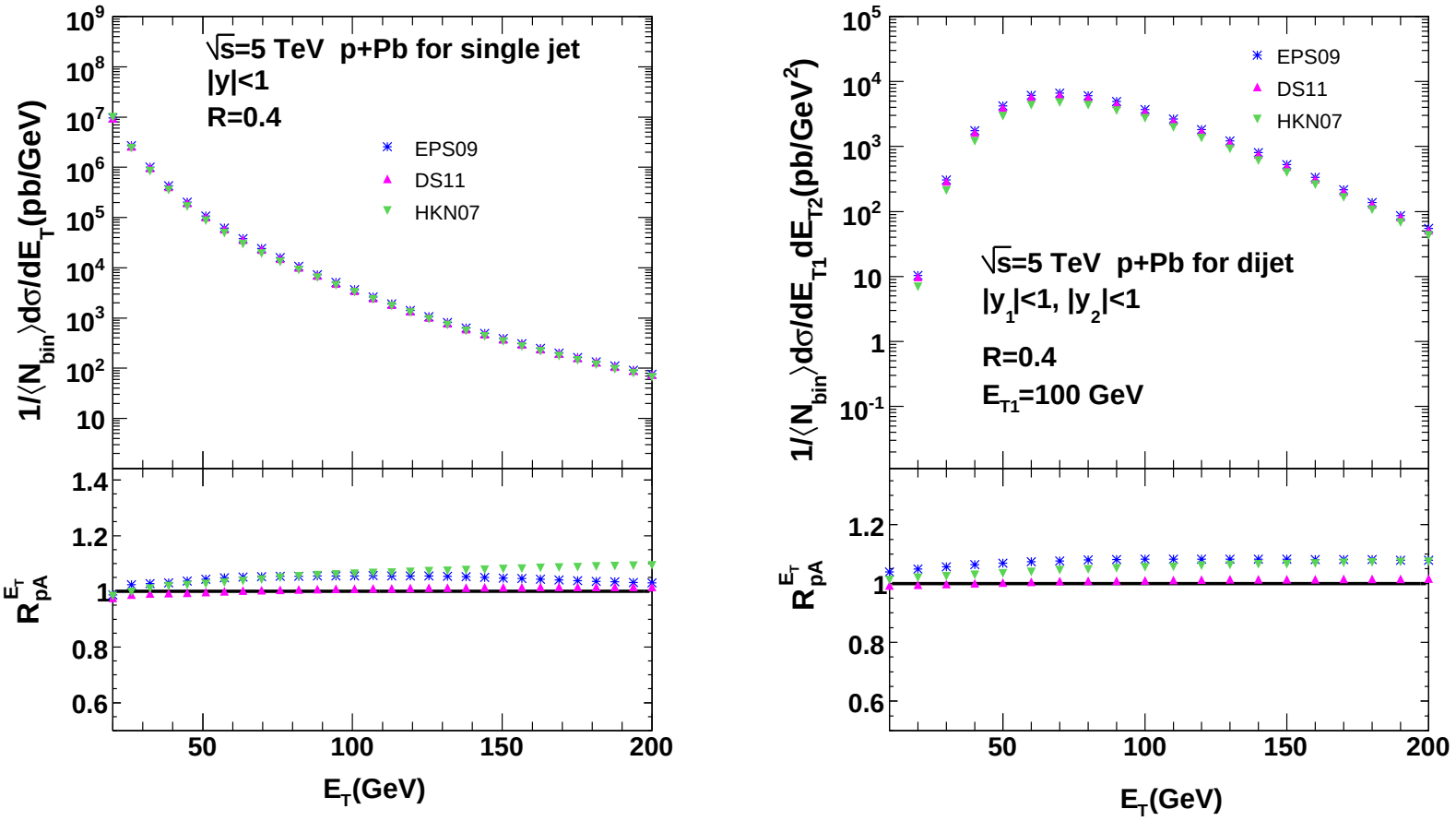

Figure 16: The inclusive jet spectra (left) and dijet E_T spectra with fixed energy $E_{T1} = 100$ GeV (right) in p+Pb collisions at $\sqrt{s} = 5$ TeV and the nuclear modification factors with three sets of nPDFs. Courtesy of Zhang *et al.*.

Azimuthal Decorrelation of Dijets

Dijet cross section for $x_1 \simeq 1$ (DGLAP density), $x_2 \ll 1$ (unintegrated gluon density)

$$\frac{d\sigma}{dy_1 dy_2 dp_{T1} dp_{T2} d\Delta\phi} = \sum_{a,c,d} \frac{p_{T1} p_{T2}}{8\pi^2 (x_1 x_2 s)^2} \mathcal{M}_{ag\to cd} x_1 f_{a/A}(x_1, \mu^2)\, \phi_{g/B}(x_2, k_T^2) \frac{1}{1+\delta_{cd}}$$

$k_T^2 = p_{T1}^2 + p_{T2}^2 + 2 p_{T1} p_{T2} \cos\Delta\phi$, $\Delta\phi$ is azimuthal distance between jets

Jet suppression (decorrelation) at $\Delta\phi \sim \pi$ due to saturation effects at large A

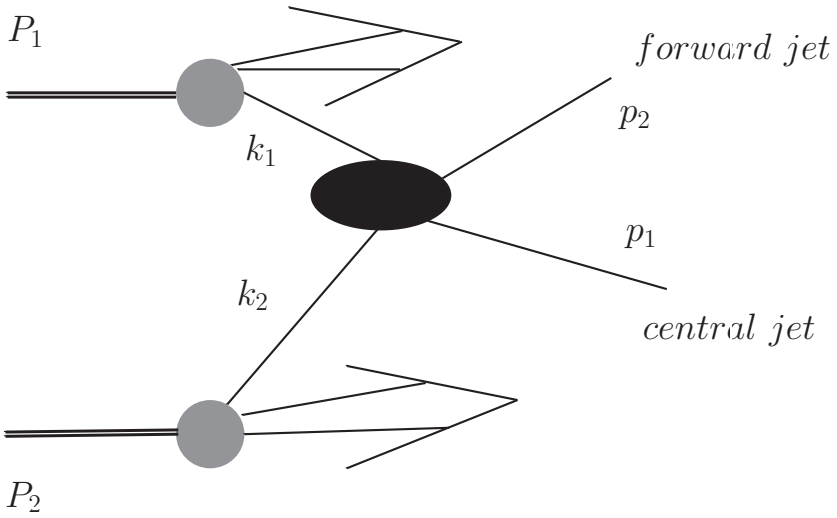

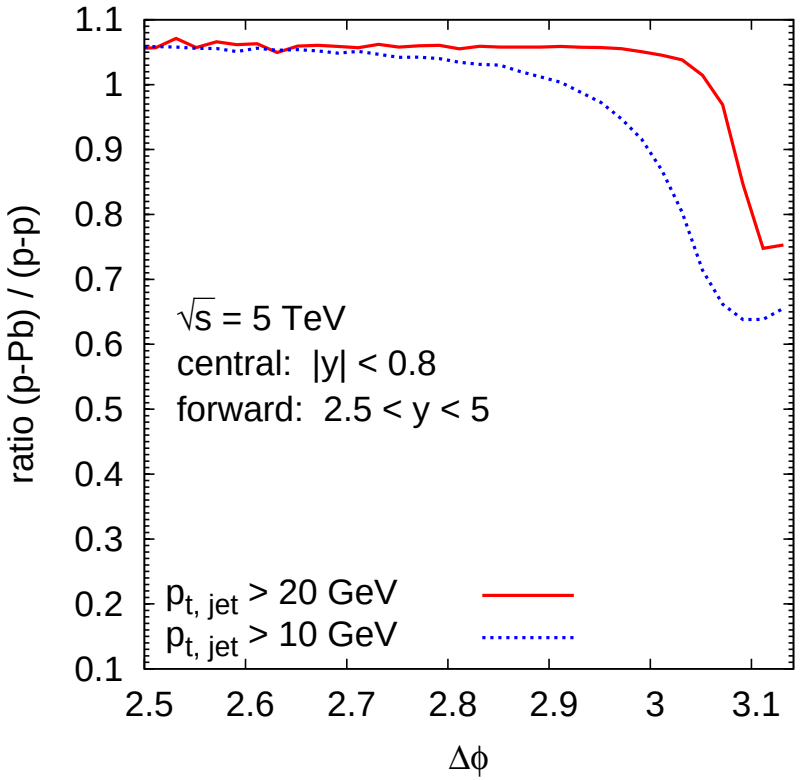

Figure 17: (Left) Jet production in the forward (assuming the proton moves toward positive rapidity) region in hadron-hadron collisions. (Right) Ratio of differential cross sections for central and forward dijet production at $\sqrt{s} = 5$ TeV as a function of the azimuthal distance between the jets, $\Delta\phi$, for pp and p+Pb collisions with two different cuts on the jets p_T. Courtesy of Kryzstof Kutak.

Photons

Direct Photon Production in pQCD

Direct photon spectra for pp compared to p+Pb

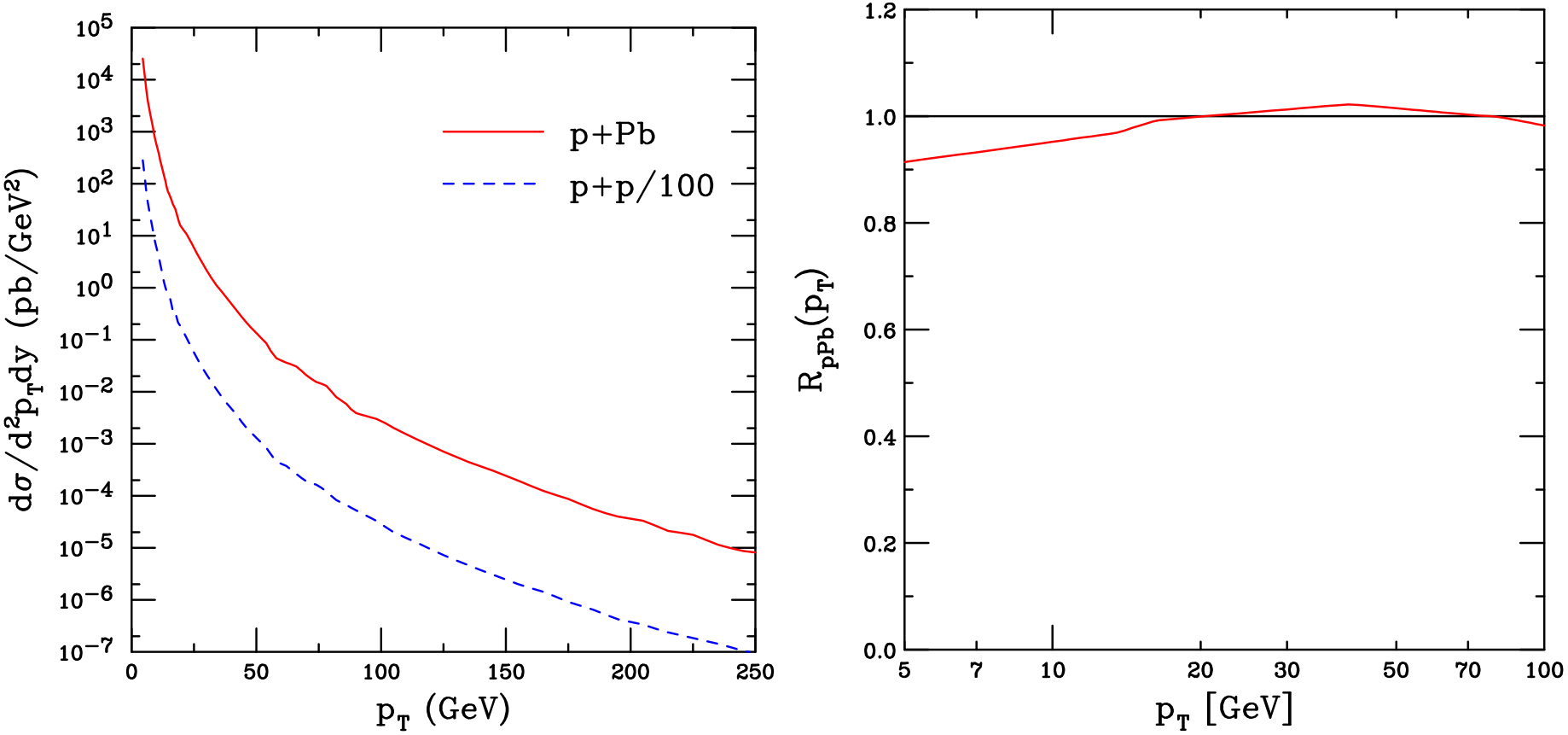

Figure 18: **(Left) The direct photon p_T distribution at $y = 0$ in the lab frame. The $p+p$ distribution is scaled down by two orders of magnitude. The p+Pb cross section is normalized to one proton-nucleon collision. An isolation cut of $E_T < 5$ GeV for hadronic energy within a $R = 0.4$ cone has been imposed. The spectra are shown in the laboratory frame of the collisions. In particular, in the lab frame the spectrum is for $y_{\rm lab} = 0$ for pp and $y = 0.47$ (in the direction of the proton) for p+Pb. The calculations were performed employing jetphox (Catani *et al.*) with EPS09 for the parton densities. (Right) The corresponding modification factor $R_{p\rm Pb}(p_T)$. Note the logarithmic p_T scale. Courtesy of R. Fries.**

Enhanced Dijet and Photon+Jet Broadening

Transverse momentum imbalance, $\mathbf{q_T = p_{T_1} + p_{T_2}}$

Broadening quantified by difference $\Delta\langle q_T^2\rangle = \langle q_T^2\rangle_{hA} - \langle q_T^2\rangle_{hp}$, double parton scattering from initial or final state, T^I and T^F are twist-4 correlation functions

$$\Delta\langle q_T^2\rangle = \left(\frac{8\pi^2\alpha_s}{N_c^2-1}\right)\frac{\sum_{a,b} f_{a/p}(x')\left[T^{(I)}_{b/A}(x)H^I_{ab\to\gamma d}(\hat{s},\hat{t},\hat{u}) + T^{(F)}_{b/A}(x)H^F_{ab\to\gamma d}(\hat{s},\hat{t},\hat{u})\right]}{\sum_{a,b} f_{a/p}(x')f_{b/A}(x)H^U_{ab\to\gamma d}(\hat{s},\hat{t},\hat{u})}$$

$$T^{(I)}_{q/A}(x) = \int\frac{dy^-}{2\pi}e^{ixp^+y^-}\int\frac{dy_1^-dy_2^-}{2\pi}\theta(y^- - y_1^-)\,\theta(-y_2^-)\frac{1}{2}\langle p_A|F_\alpha{}^+(y_2^-)\bar{\psi}_q(0)\gamma^+\psi_q(y^-)F^{+\alpha}(y_1^-)|p_A\rangle$$

$$T^{(I)}_{g/A}(x) = \int\frac{dy^-}{2\pi}e^{ixp^+y^-}\int\frac{dy_1^-dy_2^-}{2\pi}\theta(y^- - y_1^-)\,\theta(-y_2^-)\frac{1}{xp^+}\langle p_A|F_\alpha{}^+(y_2^-)F^{\sigma+}(0)F^+_\sigma(y^-)F^{+\alpha}(y_1^-)|p_A\rangle$$

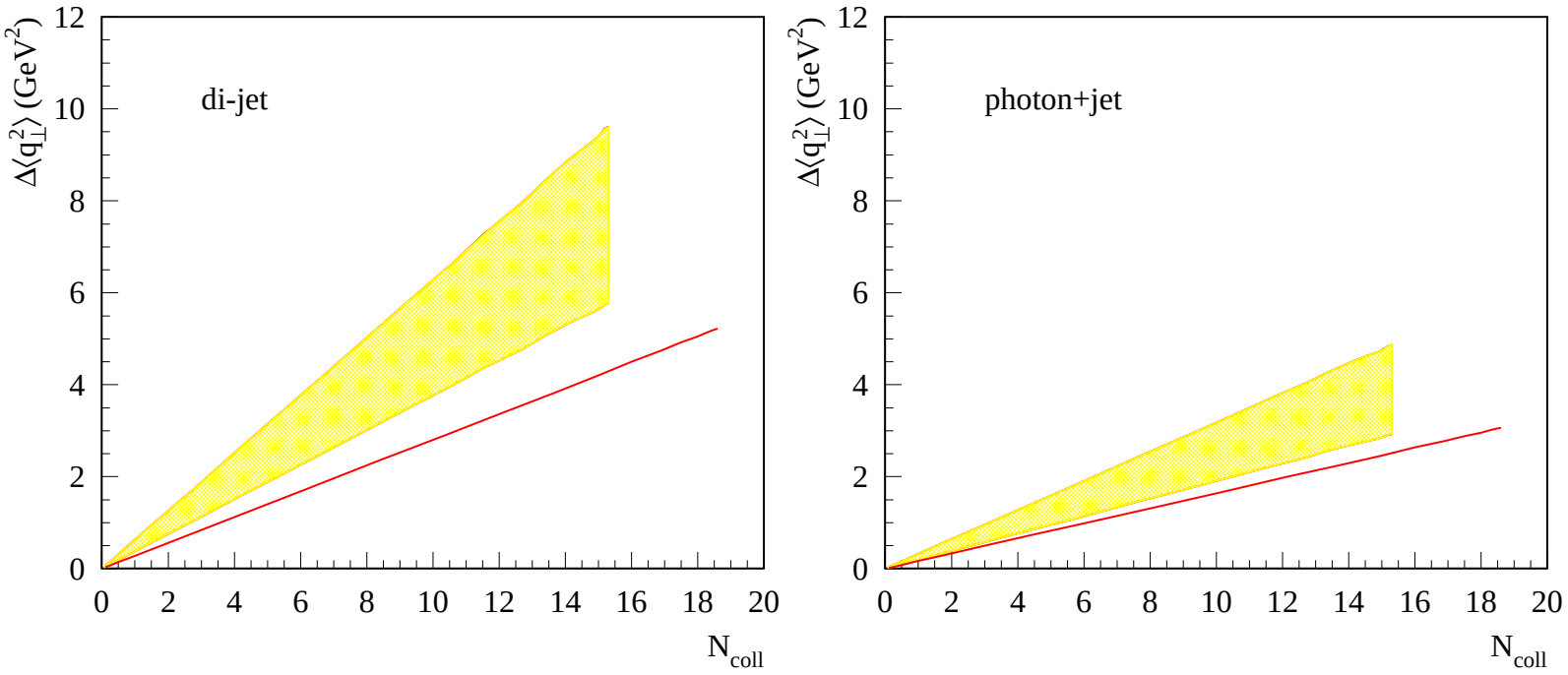

Figure 19: Nuclear broadening $\Delta\langle q_\perp^2\rangle$ for dijet (left) and photon+jet (right) production in pA collisions as a function of $N_{\rm coll}$. Fixed rapidity $y_1 = y_2 = 2$ is used for $\sqrt{s} = 5$ TeV LHC p+Pb collisions with $y_1 = y_2 = 1$ for 200 GeV d+Au collisions. At 5 TeV, the jet p_T integral is over $30 < p_T << 40$ GeV, while for RHIC, the range is $15 < p_T < 25$ GeV. The band shows a range of predictions in LHC kinematics while the red line is for RHIC. Courtesy of Ivan Vitev.

J/ψ

Pinning Down Open Charm Uncertainties by Fitting $\sigma_{c\bar{c}}$

Caveat: full NNLO cross section unknown, could still be large corrections

Employ $m = 1.27$ GeV, lattice value at $m(3\,\mathrm{GeV})$ and use subset of $c\bar{c}$ total cross section data to fix best fit values of μ_F/m and μ_R/m

Result with $\Delta\chi^2 = 1$ gives uncertainty on scale parameters; $\Delta\chi^2 = 2.3$ gives one standard deviation on total cross section

LHC results from ALICE agrees well even though not included in the fits

Same mass and scale parameters used to calculate J/ψ

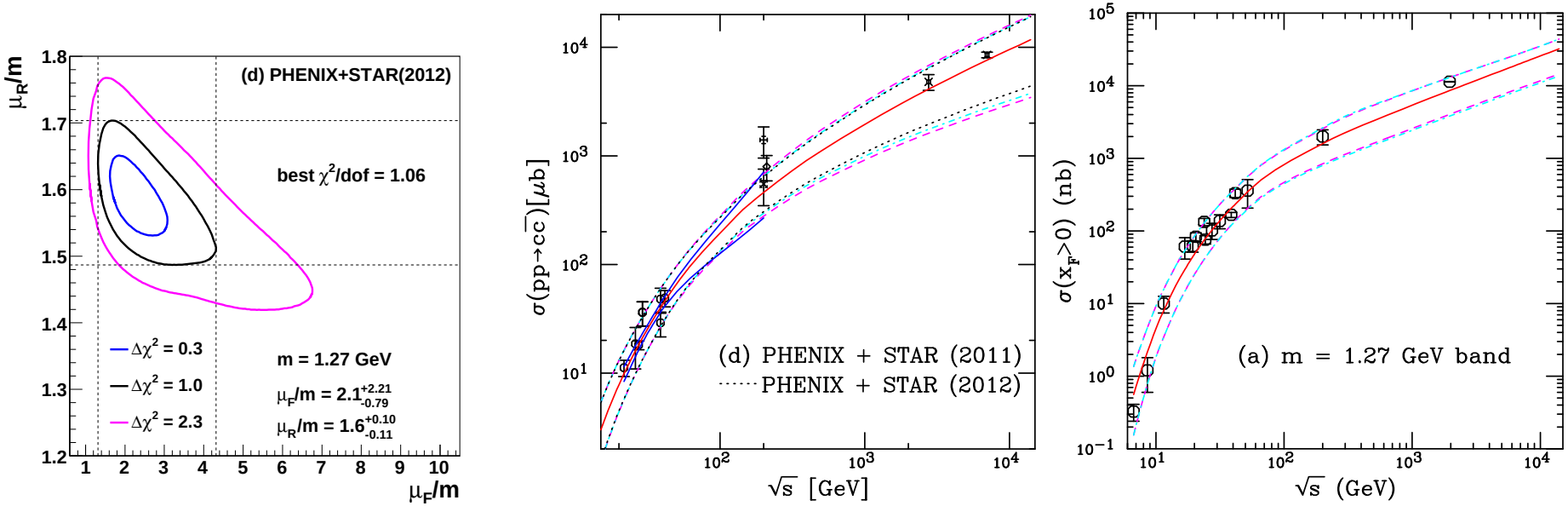

Figure 20: (Left) The χ^2/dof contours for fits including the STAR 2011 cross section but excluding the STAR 2004 cross section. The best fit values are given for the furthest extent of the $\Delta\chi^2 = 1$ contours. (Center) The energy dependence of the charm total cross section compared to data. The best fit values are given for the furthest extent of the $\Delta\chi^2 = 1$ contours. The central value of the fit in each case is given by the solid red curve while the dashed magenta curves and dot-dashed cyan curves show the extent of the corresponding uncertainty bands. The dashed curves outline the most extreme limits of the band. In addition, the dotted black curves show the uncertainty bands obtained with the 2012 STAR results while the solid blue curves in the range $19.4 \leq \sqrt{s} \leq 200$ GeV represent the uncertainty obtained from the extent of the $\Delta\chi^2 = 2.3$ contour. (Right) The uncertainty band on the forward J/ψ cross section. The dashed magenta curves

nPDF Effects on J/ψ Production

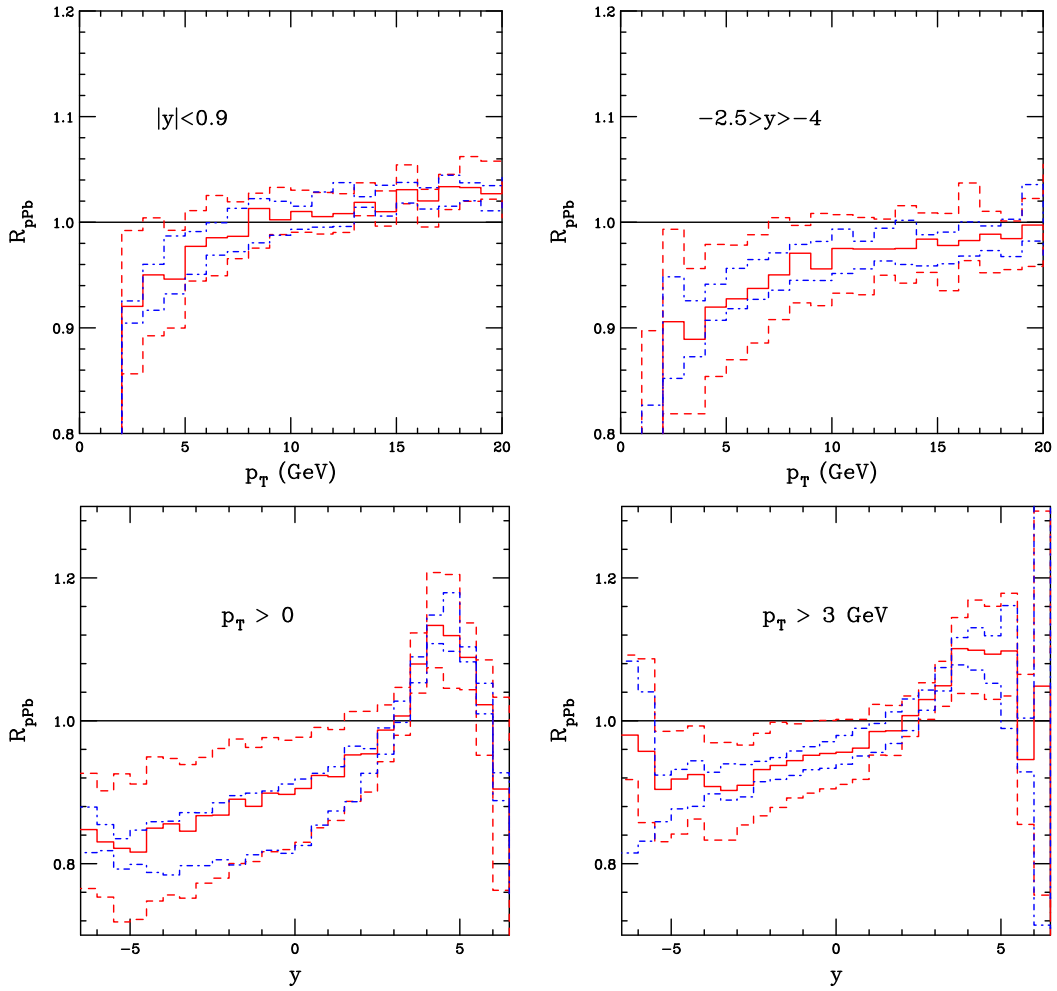

Figure 21: **The $R_{p\mathrm{Pb}}$ ratios for J/ψ as a function of p_T (top) and y (bottom). The dashed red histogram shows the EPS09 uncertainties while the dot-dashed blue histogram shows the dependence on mass and scale. The pp denominator is also calculated at 5 TeV (which isn't available experimentally) and does not take the rapidity shift in p+Pb into account. RV**

Gauge Bosons

Cold Matter Effects on W and Z Production

Isospin effects evident for W^+ and W^- production, small effect on Z

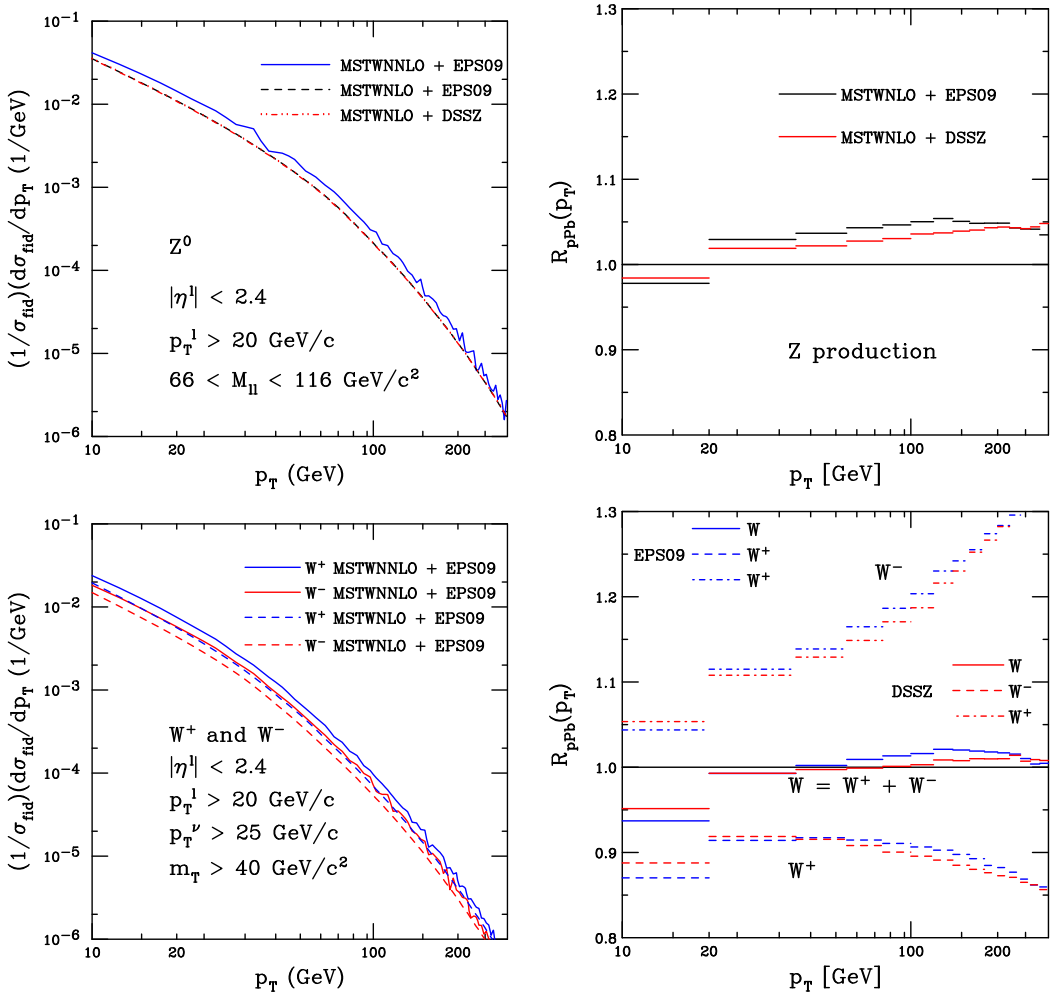

Figure 22: Normalized differential cross section (with ATLAS acceptance cuts on the leptons) $(1/\sigma_{\rm fid})(d\sigma_{\rm fid}/dp_T^Z)$ and $R_{p\rm Pb}$ for Z (top) and W (bottom) boson production. In the case of W production, $\sigma_{\rm fid}$ is the sum $W = (W^+ + W^-)$ in the fiducial phase space and p_T^W is the transverse momentum of the W^+ or W^-. Courtesy of Zhang *et al.*.

Differences in W Charge Asymmetry in pp and p+Pb

Significant difference in W^+ and W^- rapidity distributions due to p+Pb vs pp
Little difference whether calculation is NLO or NNLO

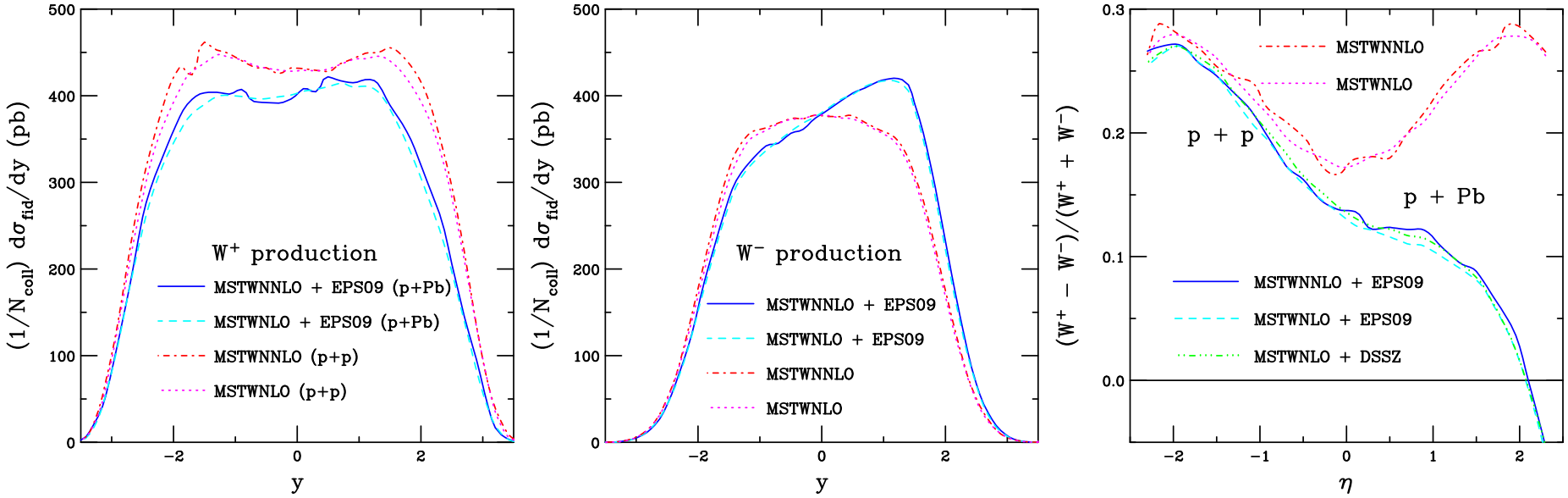

Figure 23: The W^+ (left) and W^- (center) rapidity distributions. (Right) The charge asymmetry $(N_{W^+} - N_{W^-})/(N_{W^+} + N_{W^-})$ as a function of the charged lepton pseudorapidity for W boson productions in both $p + p$ and p+Pb collisions at 5 TeV. Courtesy of Zhang *et al.*.

Broadening of Vector Boson Production

Quarkonium broadening much larger than W and Z broadening

$$\Delta\langle q_T^2\rangle_{\rm HQ}^{\rm CEM} = \left(\frac{8\pi^2\alpha_s}{N_c^2-1}\,\lambda^2\,A^{1/3}\right)\frac{(C_F+C_A)\,\sigma_{q\bar{q}}+2\,C_A\,\sigma_{gg}+\Delta\sigma_{gg}}{\sigma_{q\bar{q}}+\sigma_{gg}} \approx 2\,C_A\left(\frac{8\pi^2\alpha_s}{N_c^2-1}\,\lambda^2\,A^{1/3}\right)$$

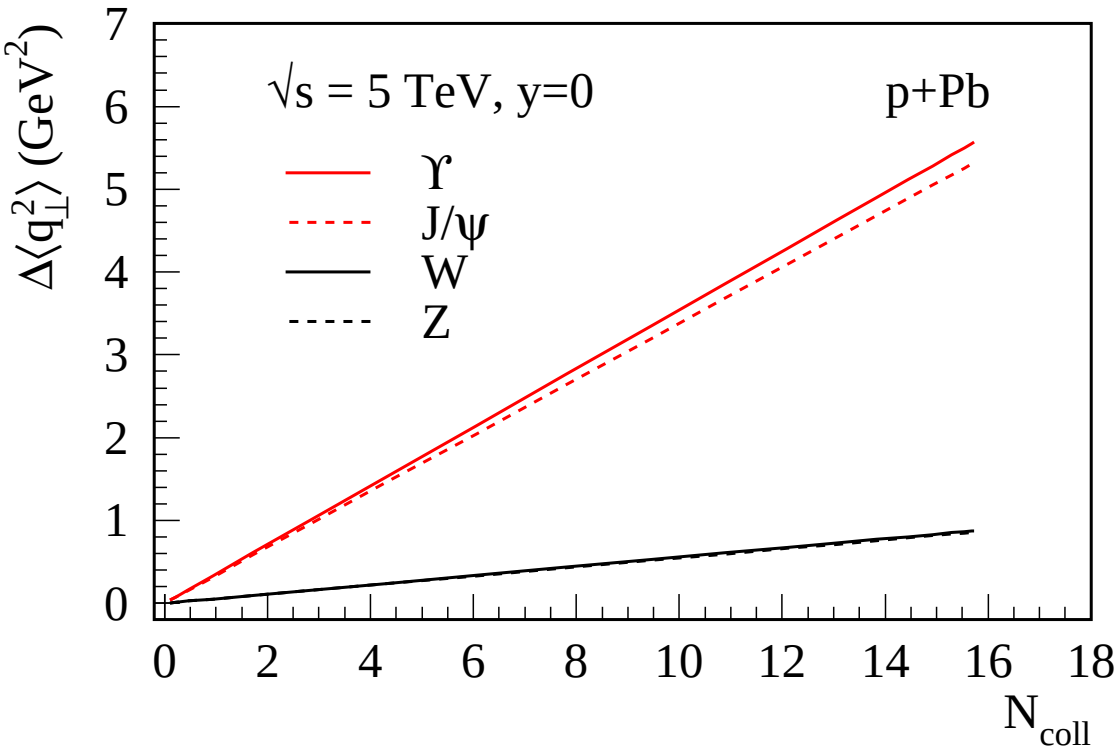

Figure 24: The transverse momentum broadening of vector boson production in p+Pb collisions at $y = 0$, shown as a function of $N_{\rm coll}$. The Υ (red solid), J/ψ (red dashed), $W^{\pm}$ (black solid), and Z^0 (black dashed) results are given. Courtesy of Qiu *et al.*.

Summary

- p+Pb run at LHC will provide interesting studies of cold matter effects in a new energy regime
- These predictions will soon be tested (if they haven't been addressed by the test run)
- Thanks again to everyone who provided predictions